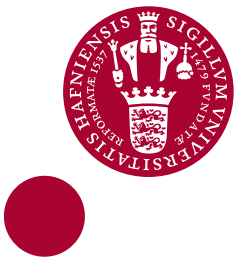

A physical model of the proton radiation belts of Jupiter inside Europa's orbit

Nénon, Quentin; Sicard, Angelica; Kollmann, Peter; Garrett, Henry B. ; Sauer, Stephan P. A.; Paranicas, Chris

Published in:
Journal of Geophysical Research: Space Physics

DOI:
10.1029/2018JA025216

Publication date:
2018

Document version
Peer reviewed version

A physical model of the proton radiation belts of Jupiter inside Europa's orbit

Q. Nénon[1], A. Sicard[1], P. Kollmann[2], H. B. Garrett[3], S. P. A. Sauer[4] and C. Paranicas[3]

[1] ONERA, The French Aerospace lab, Toulouse, France

[2] The John Hopkins University, Applied Physics Laboratory, Laurel, USA

[3] Jet Propulsion Laboratory, California Institute of Technology, Pasadena, CA, USA

[4] University of Copenhagen, Department of Chemistry, Copenhagen, Denmark

Key points

- A global physical model of the proton radiation belts of Jupiter inward of the orbit of Europa is presented
- Observed two orders of magnitude flux depletions in MeV proton fluxes near Io are not from direct interactions with the moon or its torus
- Resonant interaction with low frequency electromagnetic waves is modeled and likely to be dominant near Io's orbit

Abstract

A physical model of the Jovian trapped protons with kinetic energies higher than 1 MeV inward of the orbit of the icy moon Europa is presented. The model, named Salammbô, takes into account the radial diffusion process, the absorption effect of the Jovian moons, and the Coulomb collisions and charge exchanges with the cold plasma and neutral populations of the inner Jovian magnetosphere. Preliminary modeling of the wave-particle interaction with Electromagnetic Ion Cyclotron (EMIC) waves near the moon Io is also performed. Salammbô is validated against in-situ proton measurements of Pioneer 10, Pioneer 11, Voyager 1, Galileo Probe, and Galileo Orbiter. A prominent feature of the MeV proton intensity distribution in the modeled area is the two orders of magnitude flux depletion observed in MeV measurements near the orbit of Io. Our simulations reveal that this is not due to direct interactions with the moon or its neutral environment but results from scattering of the protons by EMIC waves.

1. Introduction

Physics-based models of radiation belts are very useful tools to forecast trapped energetic charged particle fluxes at Earth, Saturn and Jupiter. Indeed, they can contribute to a data assimilation effort around Earth (Koller et al., 2007; Shprits et al., 2007; Bourdarie and Maget, 2012), help to predict fluxes in unexplored regions of Saturn (Kollmann et al., 2015) or complement empirical models where in-situ measurements are limited to specify the harsh environment of Jupiter (Sicard-Piet et al., 2011). At Jupiter, while physical models of the trapped electrons exist (Sicard et al., 2004; Santos-Costa and Bolton, 2008; Woodfield et al., 2014; Kita et al., 2015; Nénon et al., 2017), no physical model of the trapped protons has already been developed, even though this particle population represents a major threat to satellites (Garrett et al., 2017).

On the Space Science side, physical models enable to understand the origin, morphology and time-dynamics of the radiation belts. Regarding trapped protons around gas giants, Santos-Costa et al. (2003) and Kollmann et al. (2013) proposed models around Saturn and identified the following key processes: radial diffusion, absorption by the moons and dense rings, charge exchange and energy loss with neutral particles and small ring grains and proton source by Cosmic Ray Albedo Neutron Decay. Among the very important radiation belt physical processes, wave-particle interaction is a universal physical process shaping the electron radiation belts of Earth (see for e.g. Horne et al., 2016), Jupiter (Woodfield et al., 2014; Nénon et al., 2017), and maybe Saturn (Menietti et al., 2015), consistent with saturated electron belts for Earth and Jupiter in regard with the Kennel-Petschek limit (Kennel and Petschek, 1966) discussed by Mauk and Fox (2010). One may wonder whether the resonant interaction also shapes the proton radiation belts of Jupiter, as expected in regard with the Kennel-Petschek limit (Mauk, 2014), and how similar or different the origin of the proton radiation belts of Jupiter is compared with the terrestrial and kronian ones.

A physical model of the proton radiation belts of Jupiter is proposed in this manuscript. It relies on the experience developed at ONERA through the model family named Salammbô (Beutier et al., 1995; Santos-Costa and Bourdarie, 2001; Sicard and Bourdarie, 2004;

Lorenzato et al., 2012; Nénon et al., 2017) and will simply be referred as "Salammbô" hereafter. A focus is given in this study to protons with kinetic energies higher than 1 MeV, as is done in the empirical model proposed by Garrett et al. (2017). Lower energy protons are modeled in order to address the 1 MeV fluxes anywhere inside the orbit of Europa but not directly validated against in-situ observations. Future work may focus on the development of a lower energy Salammbô-Jupiter-proton model. The modeling principle is presented in section 2. In-situ measurements used to validate the model are then presented and discussed in section 3. The modeling of the effect of all the physical processes introduced in the Salammbô model is detailed in section 4 and the outer boundary condition imposed near the orbit of Europa (L=9.5) is mentioned in section 5. Predictions of the model are documented in section 6 and validated against observations in section 7, where the possible role of charge exchange with the Io gas torus and resonant interactions with Electromagnetic Ion Cyclotron waves are discussed. Finally, our findings are summarized in section 8.

2. Modeling principle and simulation

The modeling principle adopted in this study is the same as Nénon et al. (2017), where we modeled Jupiter's electron belts. Trapped protons gyrate around a guiding center (a motion that is associated with the first adiabatic invariant (Schulz and Lanzerotti, 1974)), which bounces along the magnetic field line between two mirror points (second invariant), and experiences an azimuthal drift (third invariant). The bounce and drift motions of the guiding center define a drift shell which is described by the McIlwain parameter L and the equatorial pitch-angle α_{eq}.

The radiation belt proton distribution may be described with three coordinates if the phases associated to the three adiabatic invariants are mixed (Schulz and Lanzerotti, 1974). We use in this study the following set of three coordinates: kinetic energy E_k, sine of the equatorial pitch-angle $y = \sin(\alpha_{eq})$ and the McIlwain parameter L. The same magnetic field model as Nénon et al. (2017) is used: the internal field model O6 (Connerney, 1993) is combined with the current sheet model proposed by Khurana (1997).

The proton distribution is then governed by a diffusion equation which is detailed in Appendix A of Nénon et al. (2017) for the trapped electrons. In their last equation, the friction, absorption and diffusion coefficients represent the physical processes acting on the trapped particles and violating the three adiabatic invariants, such as radial diffusion, moon sweeping, charge exchange, Coulomb collisions, or interactions with low-frequency electromagnetic waves (see section 4).

The diffusion equation is discretized following Nénon et al. (2017) with 88 linear steps in equatorial pitch-angle, 101 logarithmic steps in kinetic energy going from 25 keV to 250 MeV at the outer boundary at L=9.5, and 51 logarithmic steps for the McIlwain parameter ranging from 1.02 to 9.5. As in Nénon et al. (2017), the kinetic energy and equatorial pitch-angle grids defined at L=9.5 are transported inward by conserving the first and second adiabatic invariants. Figure 1 shows the minimum kinetic energy simulated by the Salammbô grid using the lower kinetic energy boundary of 25 keV at L=9.5. Our model is therefore not able to

predict the distribution of 1 MeV trapped protons inside L=3 but can account for 15 MeV protons anywhere inside L=9.5.

The diffusion equation is finally solved with an explicit numerical scheme which imposes that the kinetic energy and equatorial pitch angle cross diffusion terms should be neglected, as in Nénon et al. (2017).

3. In-situ measurements

The Pioneer 10 (Jupiter flyby in 1973), Pioneer 11 (1974) and Voyager 1 (1979) missions successfully measured in-situ fluxes of the radiation belt protons inside the orbit of Europa during their respective fly-bys. In addition to these snapshots, the Galileo mission entered the Jovian magnetosphere in December 1995 and released an atmospheric probe, hereafter referred as the "Galileo Probe". The "Galileo Orbiter" remained within the Jovian radiation belts for 35 more orbits and provides an extensive survey of the belts. The Galileo survey has a limited coverage inside the orbit of Europa as the spacecraft only passed rarely in this region. Also the used instrument suffered from contamination so that not all data is directly usable. More recently, Juno arrived in polar orbit around Jupiter in July 2016 (Bolton et al., 2017). Figure 2 shows the trajectory in a magnetic frame of the previous missions. One can note that Pioneer 11 and Juno explore higher latitudes than the other spacecraft, and therefore sampled lower equatorial pitch-angle protons.

Proton measurements obtained in our region of interest and for kinetic energies greater than or close to 1 MeV are discussed hereafter. A particular attention is given to possible contamination issues. The goal of this section is to provide Salammbô with as-reliable as-possible proton measurements to validate the model for L<9.5.

The University of California – San Diego Trapped Radiation Detector (TRD) onboard Pioneer 10 and Pioneer 11 has been designed to measure integral fluxes of protons with kinetic energies higher than 80 MeV (>80 MeV hereafter) with its M3 channel.

The Pioneer 10 TRD M3 measurements are discussed by Fillius and McIlwain (1974). The measurements suffered contamination by penetrating electrons but corrections of the M3 fluxes are proposed by Fillius and McIlwain (1974) to provide a reliable measurement of >80 MeV protons inside Io's orbit. The correction also provides an estimate of the counts or fluxes that can be attributed to electron contamination along the Pioneer 10 trajectory.

The Pioneer 11 TRD M3 measurements can be found in Fillius et al. (1975) but have not been corrected for electron contamination. The counts or fluxes which can be attributed to electron contamination in the Pioneer 10 TRD M3 measurements are close or a bit higher than the fluxes measured by Pioneer 11 TRD M3. In addition, Krimigis and Armstrong (1982) have compared the Pioneer 11 TRD M3 measurements with those observed by Voyager 2 and propose that the fluxes measured by M3 at Saturn are overestimated by a factor of 3. The M3 Pioneer 11 channel is therefore considered in our study as severely contaminated by the electrons and we refrain from using it.

The University of Chicago Charged Particle Instrument (CPI) experiment includes a Fission Cell to measure >35 MeV proton fluxes. Fluxes measured by Pioneer 10 are available in Simpson et al. (1974) and those measured by Pioneer 11 in Simpson et al. (1975). However, Simpson et al. (1974) have shown that the measurements might be contaminated by electrons and heavy ions. Krimigis and Armstrong (1982) have shown that the Pioneer 11 CPI >35 MeV fluxes measured at Saturn are a factor 50 higher than the Voyager 2 measurements and suggest that this observation is highly contaminated and not reliable. We therefore do not use in the present study the Pioneer 10 and 11 CPI Fission Cell measurements, as a precaution.

The Pioneer 10 and 11 Cosmic Ray Telescope (CRT) developed by the NASA Goddard center and the New Hampshire University enables to measure two proton energy ranges: 1.2 to 2.1 MeV and 14.8 to 21.2 MeV. The Pioneer 10 CRT measurements considered here are from Trainor et al. (1974) and the Pioneer 11 ones from Trainor et al. (1975). These measurements have been corrected for the dead-time and contamination issues, so that they are considered as reliable in this study.

The Pioneer 11 Geiger Tube Telescope (GTT) experiment developed by the University of Iowa measured 0.5 to 3.6 MeV protons, can be found in Van Allen et al. (1975), and are considered as reliable.

Voyager 1 and the Low Energy Charged Particle (LECP) experiment (Krimigis et al., 1977), channel PSA3, provides us with 15-minutes averaged measurements of protons with kinetic energies between 16.3 and 26.2 MeV. This energy pass-band is given by the website of the "Fundamental Technologies" (FTECS) company: http://voyager.ftecs.com/ and is considered as the best estimate of the energy passband of PSA3 available (private discussion with S. M. Krimigis, Principle Investigator of the LECP experiment). The count rates of PSA3 are from the NASA Planetary Data System and we use a geometric factor of $0.4935\ cm^2.sr$, provided by the FTECS website, to convert the count rates to omnidirectional integral fluxes.

The Energetic Particle Investigation (EPI) onboard the Galileo Probe (Fischer et al., 1992) provides a unique dataset of electron, proton, and heavy ions measurements in the innermost part of the Jovian radiation belts. Three channels are of interest for our proton model, namely the channels P1, P2 and P3. However, as pointed out by Fischer et al. (1996), these channels do not discriminate very well particle species. We use in this study the geometric factors derived in the Ph.D. thesis of Eckhard Pehlke (Pehlke, 2000), which were computed after the first publication of Fischer et al. (1996) and are the best estimates of the detector responses we have (private discussion with L. J. Lanzerotti, Principle Investigator of EPI). Appendix A gives the geometric factors of P1, P2, and P3 in response to electrons, protons, and alpha particles (He^{2+}) extracted from Pehlke (2000). We also give in Appendix A a method to estimate the counts which might be attributed to alpha particles in P1, P2, and P3 from the measurements obtained by the channel HE of EPI. Finally, the electron model of Nénon et al. (2017) is used to compute the count rates of P1, P2, and P3 which might be attributed to trapped electrons. Appendix A also details how predicted counts are proposed from our electron and proton models taking into account the energy-dependent geometric factors.

Measurements of trapped protons by the Galileo Orbiter mission come from the Energetic Particle Detector experiment (EPD) (Williams et al., 1992). It comprises two bi-directional detectors, respectively named the Low Energy Magnetospheric Measurement System (LEMMS) and the Composition Measurement System (CMS). Only two channels of EPD actually observe protons with kinetic energies higher than 1 MeV (Mauk et al., 2004, table A1) and are therefore of interest for our study: LEMMS/B0 which observes protons with kinetic energies from 3.2 to 10.1 MeV (Jun et al., 2002) and CMS/TP3 which measures 0.54-1.14 MeV protons (Mauk et al., 2004).

Onboard the Juno spacecraft, the Jupiter Energetic particle Detector Instrument (JEDI) investigation observes trapped protons with kinetic energies up to around 2 MeV (Mauk et al., 2013). Kollmann et al. (2017) give measurements of 1.1 MeV protons observed during Perijove 1 on the 27th of August 2016. The trajectory of Juno is provided by the university of Iowa website: http://www-pw.physics.uiowa.edu/~jbg/juno.html. Salammbô will not be validated against the JEDI measurements in this study as the equatorial pitch-angle grid of the model is not sufficiently refined for the Juno trajectory. Indeed, according to the magnetic field model we use, Juno measures a few degrees in equatorial pitch angle away from the loss cone in our region of interest, what is not resolved by the currently used grid. Future work will propose a refined computation grid for the Salammbô-electron and proton models in order to address the Juno measurements. However, one can note from the Figure 2 of Kollmann et al. (2017) that the 1.1 MeV proton fluxes suffer of a depletion of around a factor 100 near the field lines with L=6, consistent with what has been observed at this energy by Pioneer 10, Pioneer 11, and Galileo (see section 6).

Table 1 summarizes the proton in-situ measurements used to validate Salammbô.

4. Modeling the effect of the physical processes

4.1.Radial diffusion

Radial diffusion in the inner magnetosphere of Jupiter might be driven by neutral winds in the ionosphere of the planet (Brice and McDonough, 1973; Miyoshi et al., 1999; Santos-Costa et al., 2008; Tsuchiya et al., 2011; Kita et al., 2015) or by electric fields in the Io torus (Bespalov and Savina, 2016; Murakami et al., 2016).

As discussed in Nénon et al. (2017), the radial diffusion coefficient of trapped particles inside Europa's orbit is poorly known. We use in this study a simple parametric form that does not depend on the particle kinetic energy or equatorial pitch-angle:

$$D_{LL} = 10^{-10} L^4 \, s^{-1}$$

The adopted radial diffusion coefficient will be validated in section 7 and possible kinetic energy dependencies discussed in section 8. One can note that our radial diffusion coefficient is close to the one used by Nénon et al. (2017) for the trapped electrons. This is reasonable since at Saturn, which has a similar magnetosphere as Jupiter, proton and electron radial diffusion coefficients were found to be similar (Kollmann et al., 2013).

4.2 Cosmic Ray Albedo Neutron Decay (CRAND)

At Earth, CRAND due to Galactic Cosmic Ray (GCR) protons nuclear interactions with the atmosphere is the main source of >10 MeV protons in the inner terrestrial radiation belt (Hess, 1959; Selesnick et al., 2013). At Saturn, CRAND from nuclear interactions with the rings is the main source of >5 MeV trapped protons (Cooper, 1983; Kollmann et al., 2013). CRAND from the Jovian atmosphere or rings might therefore be a source of trapped protons at Jupiter. However, this source is neglected in this study, for three main reasons:

- Section 6 will show that there is no evidence of CRAND in the proton measurements close to the planet. Simpson et al. (1975) and Kollmann et al. (2017) also do not find any evidence of CRAND, and therefore argue that the process is expected to be weak at Jupiter.
- The magnetic field of Jupiter has a dipole moment respectively 20000 times and 34 times larger than the one of Earth and Saturn and is therefore a stronger deflecting shield against GCR protons. Indeed, for instance, a GCR proton requires a kinetic energy of at least 1000 GeV to access the Jovian atmosphere near the magnetic equator, as computed under the magnetic dipole approximation with the formula derived by Störmer (1955). The GCR flux on the Jovian atmosphere would therefore be way less important than what is found near Earth or Saturn where GCR protons need an energy of 17 GeV to get close to the planets, so that we may speculate that the CRAND source at Jupiter is way smaller.
- Very energetic trapped protons near Earth (typically >10 MeV) may only be supplied by CRAND because inward adiabatic transport does not energize them to the observed energies. However, Jupiter's field is strong enough and its magnetosphere extended enough that radial diffusion of protons with energies as low as 300 keV from the orbit of Europa to L=2 is a source of 80 MeV protons there. Neglecting CRAND in our study therefore means that the GCR induced source is neglected against the radial diffusion source. At Saturn, the only way to produce energetic protons inward of the strongly absorbing moons and rings is CRAND. At Jupiter, there are no absorbers that work that efficiently because of the tilt of the magnetic field, so that there is no need for CRAND to explain the presence of MeV protons inward of the Jovian moons orbits.

Our assumption of neglecting CRAND is justified by the fact that the model intensities either are in agreement with the observations or tend to overestimate the proton fluxes, even in the regions closest to Jupiter (see section 7). Therefore, there is no need for an additional source like CRAND that would increase the intensities even more.

4.3 Sweeping effect of the moons

The trapped protons may impact the volcanic moon Io, which orbits at 5.9 Rj (1 Rj = 71492 km) from the center of Jupiter or the inner moons Thebe (3.1 Rj), Amalthea (2.5 Rj), Adrastea (1.8 Rj), and Metis (1.8 Rj). We assume that these moons are insulated bodies and simply absorb the impacting proton that is therefore lost from the radiation belts. The sweeping effect of the moons is modeled with a loss term $\frac{1}{\Gamma}$ in s^{-1} numerically calculated following the method detailed by Santos-Costa and Bourdarie (2001). However, their method

assumes that the gyroradius of the trapped particle is small compared to the size of the moons, which have a diameter of 3630 km (Io), 116 km (Thebe), 250 km (Amalthea), 20km (Adrastea) and 60 km (Metis). This is not true anymore for trapped protons, so that the gyroradius effect is taken into account in this study, following Paonessa and Cheng (1985). Figure 3 shows the absorption area of a moon when taking into account the proton gyroradius.

From Figure 3, we approximate the absorption area by a sphere with a diameter D given by:

$$\begin{cases} D = D_{moon} + 2 * r_g \; if \; r_g \leq \frac{D_{moon}}{2} \\ D = 2 * \sqrt{2 * D_{moon} * r_g} \; if \; r_g \geq \frac{D_{moon}}{2} \end{cases}$$

For instance, the moon Thebe which has a geometric radius of around 55 km is seen by a 15 MeV proton with a gyroradius of 39km as an absorber body with a radius of 94km.

4.4 Effect of the dust rings

Jupiter has four very tenuous dust rings. They are believed to be populated by silicon dioxide grains created by micro-meteoroids impacts on the four inner moons Metis, Adrastea, Amalthea and Thebe (Burns et al., 1999). The grains then drift inward under the Pointyng-Robertson drag effect to create the rings. The two innermost rings are the Halo (1.25 to 1.72 Rj) and the main ring (from 1.72 to 1.82 Rj) which is the brightest one. The two external Gossamer rings produced by meteoroid impacts on Amalthea and Thebe extend respectively from 1.72 to 2.54 Rj and 1.72 to 3.11 Rj in the equatorial plane.

The effect of the rings is not included in the present model and will be the object of a future study which will discuss the effect of the rings against proton measurements (using the Salammbô model presented here) and electron in-situ measurements and synchrotron observations (using the model of Nénon et al. (2017)). However, the validation of the proposed proton model against Galileo Probe EPI measurements in section 7 shows that the main ring may have a predominant effect on >60 MeV protons close to Jupiter. We give hereafter a first calculation to further test this hypothesis.

Following Brooks et al. (2004), we assume that the main ring is composed of uniformly distributed spherical grains with a radius of $15\ \mu m$. >60 MeV protons easily go through these grains and only suffer of a kinetic energy friction $\frac{dE}{dt}$. The stopping power of the main ring is then scaled from the stopping power of the silicon dioxide with the ratio between the molecular density in the ring and the molecular density of silicon dioxide (Kollmann et al., 2015):

$$\left.\frac{dE}{dx}\right|_{ring} = \left.\frac{dE}{dx}\right|_{S_iO_2} * \frac{n_{molecule-ring}}{n_{molecule-S_iO_2}}$$

Following the method of Kollmann et al. (2015) to compute the molecular density in the ring, we finally have:

$$\frac{dE}{dt} = -v * \frac{dE}{dx}\Big|_{ring} = -v * \frac{4}{3}\pi\, r^3\, n * \frac{dE}{dx}\Big|_{S_iO_2}$$

Where r is the radius of the grains, assumed to be $15\ \mu m$, v the speed of the proton and n the grain density within the ring. This density is computed by assuming an optical depth at visible wavelength of $5.9\ 10^{-6}$ (Brooks et al., 2004) and a thickness of the ring of $200\ km$ (Brooks et al., 2004). The stopping power of silicon dioxide is given by the NIST database. The kinetic energy friction term for 60 MeV protons staying within the ring during their full drift period is finally of $-\frac{1}{E}\frac{dE}{dt} = 2\ 10^{-6}\ s^{-1}$, what is three orders of magnitude higher than the local radial diffusion coefficient at $L = 1.8$ of $D_{LL} = 10^{-9}s^{-1}$. This first calculation shows that the main ring may clearly have a strong effect on the protons observed by Galileo Probe-EPI.

4.5 Coulomb collisions with cold plasma and neutral gas torus

Trapped protons inside Europa's orbit experience elastic Coulomb collisions with:

- The free electrons of the cold plasma of the inner magnetosphere of Jupiter
- The bound electrons of the cold plasma ions
- The bound electrons of the neutral particles of the Jovian hydrogen corona and Io and Europa gas torus

The equatorial pitch-angle diffusion, i.e. the trajectory deflection, is negligible for trapped protons (Schulz and Lanzerotti, 1974). However, trapped protons suffer of subsequent kinetic energy losses that are represented with the kinetic energy loss rate $\frac{dE}{dt}$ computed as follow:

$$-\frac{dE}{dt} = \frac{4\pi}{m_{0e}v}\left(\frac{q^2}{4\pi\varepsilon_0}\right) * \left[\chi_{free} + \chi_{bound}\right]$$

Where v is the proton velocity, m_{0e} the rest mass of the electron and the χ_{free} and χ_{bound} terms give the contribution from free and bound electrons and are computed following Schulz and Lanzerotti (1974) by:

$$\chi_{free} = \langle n_e \rangle \left[1 - \frac{1}{\gamma^2} - ln\left(\frac{\lambda_D m_{0e} v}{\hbar}\right)\right]$$

$$\chi_{bound} = \sum_i Z_i \langle n_i \rangle \left[1 - \frac{1}{\gamma^2} - \ln\left(\frac{2m_{0e}c^2(\gamma^2 - 1)}{I_i}\right)\right]$$

With λ_D the Debye length evaluated at the magnetic equator, $\langle n_e \rangle$ the free electron number density averaged over the drift shell and γ the Lorentz factor. The sum in χ_{bound} is evaluated over the different ions and neutral particles with drift shell averaged number densities $\langle n_i \rangle$ and mean excitation energies I_i.

The atmosphere model is the same as Nénon et al. (2017). The cold plasma free electron and ion densities are provided by the model of Divine and Garrett (1983), which is consistent with

more recent models of the magnetodisc by Bagenal (1994), Bagenal and Delamere (2011), or Bagenal et al. (2016). Divine and Garrett (1983) also provides us with the plasma temperatures to compute the Debye length.

As in Nénon et al. (2017), the Coulomb collisions with the neutral particles of the Io gas torus are neglected against the elastic collisions with the cold plasma ions, as their densities are one order of magnitude lower than the ion ones and that the mean excitation energies are similar. However, it is not true anymore near Europa, where ion densities range from 1 to 20 cm^{-3} while neutral densities may range from 1.6 to 410 cm^{-3} (Kollmann et al., 2016), depending on the assumptions. Coulomb collisions with the neutral gas torus of Europa is still neglected in our study, and section 4.9 will show that this assumption does not impact the Salammbô results, as Coulomb collisions will remain negligible against local radial diffusion near Europa's orbit.

Sicard and Bourdarie (2004) and Nénon et al. (2017) did not take into account the Coulomb collisions with the oxygen and sulfur ions of the magnetodisc O^+, O^{++}, S^+, S^{++}, and S^{+++}. To do so, one needs the mean excitation energies I_i of the oxygen and sulfur ions. Sauer et al. (2015) computed the mean excitation energies of various atomic ions. Mean excitation energies of oxygen and sulfur ions have been computed for this study following the method detailed by Sauer et al. (2015) or Jensen et al. (2016) and are reported in Table 2.

4.6 Charge exchange with the Jovian atmosphere

Trapped protons H^+ may experience a charge exchange or a charge transfer with the neutral particles A of the Jovian atmosphere following:

$$H^+ + A \rightarrow H + A^+$$

The proton is therefore lost from the radiation belts, and the loss term is computed as:

$$\frac{1}{\Gamma} = v * \sigma * \langle n(A) \rangle$$

Where v is the speed of the proton, $\langle n(A) \rangle$ the density of neutral particles averaged on the bounce and drift motions of the trapped proton and σ the charge exchange cross section associated to the previous reaction.

For the Jovian atmosphere, only charge exchange with hydrogen atoms, the main constituent in the upper atmosphere, is taken into account in Salammbô. The density model is the same as Nénon et al (2017) and the charge exchange cross section is given by Claflin (1970).

4.7 Charge exchange with the neutral gas torus of Io and Europa

The intense volcanic activity of Io releases sulfur dioxide molecules SO_2 into space, creating a neutral gas torus mainly composed of oxygen and sulfur particles (Smyth and Marconi, 2006). A gas torus is also found near the moon Europa, created by sputtering and potentially plumes (Sparks et al., 2016) and composed of oxygen atoms and dihydrogen molecules. Charge exchange with these neutral populations may remove trapped protons from the

radiation belts. In order to evaluate this loss process, one needs to know the neutral densities and associated charge exchange cross sections.

The kinetic model of Smyth and Marconi (2006) predicts the radial extension of the Io and Europa gas torus. In our region of interest, the Io torus extends from 1 Rj to 9.5 Rj and the Europa torus from 6 Rj to 9.5 Rj, the outer boundary of our model. Figure 4 shows the geometric configuration of the two gas tori used in this study, with a constant thickness of respectively 1.4 Rj for the Io torus (Smyth and Marconi, 2006) and 2 Rj for the Europa torus (Kollmann et al., 2016). The assumption of a thickness is also necessary to derive densities from the column densities provided by Smyth and Marconi (2006).

Smyth and Marconi (2006) predict that the oxygen atom number densities dominate over the sulfur atoms ones in the Io torus. The effect of the sulfur atoms is neglected against the effect of the oxygen atoms, as the charge exchange cross sections of H^+ on O and S are similar (Varghese et al., 1985). We therefore only focus on oxygen atoms in the Io torus and their density is supposed to be uniform along a vertical axis with a radial distribution given by:

$$\begin{cases} n(\rho) = n_{max} * A_{O_1} * exp\left(B_{O_1} * \rho\right) for\ 1 \leq\ \rho \leq 6 \\ n(\rho) = n_{max} * A_{O_2} * exp\left(B_{O_2} * \rho\right) for\ 6 \leq\ \rho \leq 9.5 \end{cases}$$

Constants $A_{O_1}, A_{O_2}, B_{O_1}, B_{O_2}$ are approximating the column densities given by Smyth and Marconi (2006) and the maximum density n_{max} is let free in our simulations. UV observations of the Io torus propose a value of $n_{max} \approx 30\ cm^{-3}$, as summarized by Lagg et al. (1998). Observations of the pitch-angle distribution of energetic heavy ions suggest values of $n_{max} \approx 30\ cm^{-3}$ (Lagg et al., 1998) or $n_{max} \approx 10\ cm^{-3}$ (Mauk et al., 1998).

In the Europas torus, the densities of H_2 dominate the densities of O (Smyth and Marconi, 2006). We therefore neglect the contribution of the oxygen atoms against the dihydrogen molecules, as is done by Kollmann et al. (2016). The radial distribution of dihydrogen molecules is fitted to the column densities given by Smyth and Marconi (2006), as we did for the oxygen of the Io torus. The maximum density of H_2 is let free, and may vary from 1.6 to $410\ cm^{-3}$ (Kollmann et al., 2016).

Charge exchange cross sections of trapped protons with dihydrogen molecules of the Europa torus are found in Barnett et al. (1990). For the cross section of protons on neutral oxygen, we use the values given by Lindsay and Stebbings (2005) for kinetic energies lower than 100 keV. Varghese et al. (1985) provide values of the cross section above 800 keV. In between 100 keV and 800 keV, we extrapolate the results of Lindsay and Stebbings (2005) to fit the value reported by Varghese et al. (1985) at 800 keV. Figure 5 shows the adopted cross section. The proposed extrapolation fits very well the values reported by Varghese et al. (1985).

Finally, charge exchange with the ions of the magnetodisc ($O^+, O^{++}, S^+, S^{++}, S^{+++}$) is neglected in this study against charge exchange with the neutral atoms and molecules. This assumption is supported by the charge exchange cross sections of H^+ on the oxygen ions

computed by Fujiwara (1976), where these are two to three orders of magnitude lower than the cross sections of H^+ on neutral oxygen.

4.8 Wave-particle interaction

Low-frequency electromagnetic waves, with frequencies under the local proton gyrofrequency, may resonate with the gyromotion of trapped protons and diffuse their equatorial pitch-angle and kinetic energy (Kennel and Engelmann, 1966). These waves propagate at frequencies close to ion cyclotron frequencies and are therefore named Electromagnetic Ion Cyclotron waves, or EMIC waves. A first modeling of the effect of the EMIC waves on Jovian protons is proposed in this study. To do so, the WAve-Particle Interaction software (WAPI), which relies on the quasi-linear theory and is developed by ONERA (Sicard-Piet et al., 2014), has been used.

EMIC waves can form as a result of corotating neutral molecules from the Io torus being ionized and picked up. Strong EMIC waves were observed by the Ulysses/URAP (Unified Radio And Plasma wave) experiment near Io in 1992 (Lin et al., 1993) and by Galileo/MAG during four passes over Io (Kivelson et al., 1996; Warnecke et al., 1997; Bianco-Cano et al., 2001; Russell et al., 2001). Following these observations, we assume that the EMIC waves propagate along magnetic field lines with $5.95 \leq L \leq 6.22$, which represent one interval near Io in the L-grid of Salammbô, and their effect is neglected outside this area.

The waves have been observed to have a left-handed polarization and to propagate parallel to the magnetic field lines near the magnetic equator. It is therefore assumed in this study that the propagation angles of the EMIC waves follow a Gaussian law with a mean propagation angle of $\theta_m = 0°$, a full width at half of the maximum $\delta\theta = 30°$ and low and high cutoff angles of $0°$ and $70°$.

It is also assumed, as in Nénon et al. (2017), that wave-particle interaction in the magnetodisc, i. e. for magnetic latitudes around [-10°,+10°], dominates over the resonant interaction at higher latitudes.

Figure 1 of Bianco-Cano et al. (2001) shows EMIC waves spectral magnetic densities measured by Galileo/MAG. Very strong EMIC waves have been observed with frequencies in between the gyrofrequencies of the SO_2^+ and SO^+ ions. These waves have two to three orders of magnitude stronger spectral densities than the other observed frequencies. It is therefore assumed here that the effect of EMIC waves with frequencies between 0.4 and 0.7 Hz dominates over the effect of the other frequencies. The spectral magnetic density of the simulated EMIC waves is assumed to follow a Gaussian function, with low and high cutoff frequencies of 0.4 and 0.7 Hz, a mean frequency of 0.6 Hz and a large full width at half of the maximum of 10000 Hz. The last width enables to simulate a constant spectral magnetic density between the two frequencies of interest. The value of this constant should represent the drift-averaged density seen by trapped protons, that we tune in this study between 0 and the values observed by Galileo/MAG near Io as the occurrence rate and longitude distribution of EMIC waves in the Io torus are unknown. Galileo/MAG observations suggest that the constant should be capped by 10^2 to $10^4 nT^2.Hz^{-1}$. In our model, a value of $2\ nT^2.Hz^{-1}$ is

adopted to discuss the possible effect of EMIC waves on trapped protons. This value does not seem to be unrealistic in regard with Galileo/MAG observations.

Harmonic numbers of -5 to +5 are considered. This harmonic number range is found to be sufficient to compute the diffusion rates, as wider ranges give similar results. Finally, the cold plasma electron and ion densities are given by the model of Bagenal (1994) based on Voyager measurements at the orbit of Io.

4.9 Balance of the physical processes

The balance of the physical processes introduced in Salammbô is discussed here, in order to point out the predominant effects shaping the Jovian proton belts for kinetic energies higher than 1 MeV. A first way to estimate this balance is to have a look at the values of the absorption, friction and diffusion coefficients, normalized in s^{-1}. Figure 6 documents these coefficients and one can say, at first order, that a process is important if its coefficient is close or greater than the local radial diffusion. Conversely, a physical process with a diffusion coefficient one or two orders of magnitude lower than the local radial diffusion is not very effective.

A first result of our study is about the kinetic energies of the protons with which 0.4-0.7 Hz EMIC waves may resonate. Figure 6 panel a) shows that the strongest equatorial pitch-angle diffusion coefficients near Io are found for low equatorial pitch-angle 1 MeV protons, while higher energies may be affected at higher equatorial pitch angles. The assumed spectral magnetic density of $2\,nT^2.Hz^{-1}$ makes the 0.4-0.7 Hz EMIC waves very effective in diffusing the equatorial pitch-angle of the trapped protons, so that strong proton precipitations in the Jovian atmosphere might be expected. Kinetic energy diffusion is found to be negligible against local radial diffusion.

As seen in Figure 6, charge exchange with the neutral gas torus of Europa is a strong loss process of 100 keV protons near the icy moon, as the associated coefficient is higher than local radial diffusion, what is consistent with the data analysis of Kollmann et al. (2016). At this energy, charge exchange with neutral oxygen of the Io torus might be important near the volcanic moon but does not seem to be effective near Europa. For 1 MeV protons, charge exchange is a negligible process with the assumed maximum neutral densities, but a density in the Io torus a factor 100 higher than what has been used might change this conclusion (see section 7).

Coulomb collisions at 0.1 MeV is not affected by whether we take into account or not the elastic collisions with the ions of the magnetodisc, as the dashed blue line is superimposed with the thick blue line in Figure 6. A difference however appears at higher energies. Coulomb collisions are found to be negligible at >1 MeV against local radial diffusion. Near Europa, the Coulomb collisions coefficients are for all considered energies a few order of magnitudes lower than the local radial diffusion, what makes them negligible near the icy moon, even if Coulomb collisions with neutral particles were added. This justifies our assumption of section 4.5 on neglecting elastic collisions with neutral particles.

The strong absorption effect of the Jovian moons is noted, which gets more and more effective as the kinetic energy of the considered proton increases. It comes from the proton gyroradius, which is proportional to the square root of the energy and increases the absorption area of the moon, as discussed in section 4.3, but also from the drift period of the protons being faster at high energies, making the moon sweeping process more effective.

5. Outer boundary condition

The outer boundary condition should represent the kinetic energy spectrum and equatorial pitch-angle distribution of trapped protons at L=9.5. The equatorial omnidirectional differential kinetic energy spectrum is from the GIRE3 model (Garrett et al., 2017), which reproduces the Galileo/EPD/CMS spectra published by Mauk et al. (2004) under 1 MeV and fits the Pioneer measurements above. This spectrum is shown in Figure 7 b-d.

The equatorial pitch-angles are supposed to have near Europa's orbit a "pancake" distribution, peaked at 90°, reproduced by a sine function:

$$f\left(E_k, y = \sin\left(\alpha_{eq}\right), L = 9.5\right) = f(E_k, y = 1, L = 9.5) * \sin(\alpha_{eq})$$

Section 7 will validate the adopted outer boundary condition against in-situ measurements.

6. Salammbô predictions

Figure 7 panel a) shows predictions of the integral omnidirectional fluxes of protons by the Salammbô model in a magnetic meridian plane, using a maximum neutral density in the Io gas torus of 35 cm^{-3} and a maximum neutral density in the Europa gas torus of 410 cm^{-3}. These assumptions are not critical for the shown model output at >1 MeV. Outside of the equator, Figure 7 panel a) shows that the predicted fluxes strongly decrease near L=6. Validations in section 7 will discuss the origin of this decrease in our model, whether it is an absorption effect of Io, charge exchange with neutral particles or resonant interactions with EMIC waves.

Kinetic energy spectra predicted at the magnetic equator for various L values are then documented in panels b, c and d. For the energy spectra, several simulation results are shown, with a model which does not take into account neither charge exchange with the Io and Europa gas torus or resonant interactions with EMIC waves (panel b), one model without EMIC waves but with charge exchange with the gas torus (panel c) and the last model with charge exchange and EMIC waves (panel d).

Sharp flux drops at low energies seen in panel b-d are artifacts resulting from the minimum kinetic energy boundary condition, as discussed by Nénon et al. (2017). Real spectra are expected instead to gradually decrease to low energies due to charge exchange losses, as we discuss below. Intensities above the sharp drop-off are unaffected by the artifact.

Panel b enables to appreciate the adiabatic transport of protons: this process essentially shifts spectra at large L towards higher energy when moving inwards to smaller L. It also shows the absorption effect of Io between L=6.65 and L=5.56. No clear absorption effect of the inner

moons Thebe (between L=2.98 to L=2.38) or Metis and Adrastea (between L=2.08 to L=1.59) is seen in the equatorial and omnidirectional flux. This is a major difference to the trapped electrons that comes from the fact that protons do not experience pitch-angle diffusion by Coulomb collisions or pitch-angle frictions by synchrotron radiation. Indeed, the previous diffusion and friction would help to move equatorial protons to higher mirror latitudes where they can be swept more efficiently by the moons, making the absorption effect of the moon observable in the omnidirectional equatorial flux. The model therefore predicts that equatorial protons do not suffer of moon absorptions, what creates the elongated equatorial flux seen near the magnetic equator close to Jupiter in the >80 MeV meridian plot.

Figure 7 panel c) shows losses by charge exchange with the Io and Europa gas torus, effective for kinetic energies lower than a few hundreds keV. Strong losses due to the interaction with EMIC waves near Io can be seen in Figure 7 panel d), with a wavy pattern similar to what wave-particle interaction does on trapped electrons (Nénon et al., 2017).

7. Validation of the model against in-situ observations

The validation of the Salammbô proton model that takes into account charge exchange with the Io and Europa torus and resonant interaction with EMIC waves near Io is discussed here. Table 1 shows that in-situ flux measurements are available in three energy ranges: 1 to 3 MeV, around 15 MeV and then around >60 MeV to >80 MeV (what we call hereafter "very energetic protons"). This section presents the comparison of the proton fluxes predicted by the Salammbô model with the observations in these three energy ranges.

Predictions of the model in which the effect of EMIC waves is switched off are also shown, to discuss the effect of these waves on our predictions. A discussion on the effect of the charge exchange process is also included, in order to discuss the origin of the intense flux depletion observed near Io in 1 MeV measurements.

7.1. Validation against 1 to 3 MeV observations

Figure 8 shows the comparison of predicted fluxes with 1 to 3 MeV observations. The outer boundary condition imposed near the orbit of Europa can either be seen at L=9.5 for the Galileo plots, or at the beginning and end of our model of the Pioneer fly-bys. One can note that the Salammbô outer boundary condition understimates the 1 MeV fluxes by a factor 2 to 10 near Europa. However, the slope of the intensity change between the orbit of Europa and Io (that results mostly from adiabatic acceleration) is consistent with the measurement. Then, near Io, a two-order of magnitude flux depletion is seen in the five channels. One can note that the Salammbô model without EMIC waves do not predict this intense depletion at all, even when assuming the maximum reasonable densities in the Io and Europa tori. This means that our model clearly dismisses the absorption effect of Io or its torus as the origin of the observed flux depletion. Only when additional losses due to EMIC waves scattering protons in Jupiter's atmosphere are taken into account, the amplitude of the depletion is better reproduced, with a maximum to minimum ratio near Io of around 50. The flux depletion is therefore still underestimated but our modeling shows that EMIC waves with the frequencies and spectral magnetic densities discussed in section 4.8 might be the origin of it.

552 Our modeling effort shows that charge exchange near Europa is very effective to remove
553 protons in the energy range of hundreds of keV from the proton belts, consistent with the
554 conclusions of Kollmann et al. (2016). In principle, this depletion at relatively low energies
555 and large distances translates into a depletion in the MeV range when the protons are
556 transported inward towards the orbit of Io. However, our simulations reveal that this charge
557 exchange depletion is negligible against the sweeping effect of Io on MeV protons.

558 Regarding the Io gas torus, the maximum density of neutral oxygen is not known with
559 certainty but has been reported to be around $35\ cm^{-3}$ (see section 4.7). Even a maximum
560 density of $350\ cm^{-3}$ has no observable effect in our simulations, while Figure 9 shows the
561 effect of a maximum density of $3500\ cm^{-3}$ on the 1 MeV prediction along the trajectory of
562 Pioneer 10. One can note that this enhanced charge exchange process does not help to
563 reproduce the observed flux depletion near Io. However, it completely empties the 100 keV
564 proton belts at Io's orbit, what is seen inward of the volcanic moon in our predictions. Using
565 the charge exchange cross sections detailed in section 4.7, we therefore dismiss charge
566 transfer with the Io gas torus as a possible explanation of the observed flux depletions in 1
567 MeV measurements near the moon, independently of the neutral number density.

568 ### 7.2. *Validation against 15 MeV observations*

569 Figure 10 is similar to Figure 8 and shows the comparison between the in-situ measurements
570 around 15 MeV by Pioneer 10, Pioneer 11 and Voyager 1 and the fluxes predicted by the
571 Salammbô model in this energy range. One can note that the adopted outer boundary
572 condition is in agreement with the Pioneer 10 and Pioneer 11 measurements, what tends to
573 validate the chosen equatorial pitch-angle dependency detailed in section 5. However, the
574 outer boundary condition overestimates the Voyager 1 fluxes by a factor of 3, what might be
575 inferred to time variability or to an underestimated geometric factor of the PSA3 channel of
576 LECP. The intensity increase of trapped protons from Europa to Io is consistent with the
577 measurements. Near Io, flux depletions predicted along the Pioneer 10 outbound, Voyager 1
578 outbound, and Pioneer 11 trajectories are not affected by whether EMIC waves are introduced
579 in the model or not and are realistically predicted. These cases where the prediction is
580 independent of the effect of EMIC waves validate the adopted radial diffusion coefficient, as
581 the good match obtained between model and data only comes from the adopted boundary
582 condition (constrained by many in-situ measurements), the sweeping effect of Io (that is a
583 geometric calculation in which we trust) and the radial diffusion coefficient (the assumption
584 we validate). Pioneer 10 inbound and Voyager 1 inbound predictions are however strongly
585 affected by EMIC waves with the assumed magnetic densities (see section 4.8) and reduce the
586 intensities by about one order of magnitude relative to our model without EMIC waves. For
587 the Pioneer 10 prediction, the flux depletion with EMIC waves is overestimated, what then
588 tends to have fluxes underestimated of around of a factor 20 near perijove. While the absolute
589 values of the predicted Voyager intensities deviate from the observations, the relative
590 intensity change across Io's sweeping zone is properly predicted by the model including
591 EMIC waves. Finally, on the Pioneer 10 outbound trajectory, a flux depletion is predicted
592 near the orbit of Thebe and consistent with the observation. On Pioneer 11, effect of the
593 EMIC waves is only seen for McIlwain parameters lower than 3. The model, with or without

EMIC waves, correctly reproduces small flux depletions near the orbit of Thebe and Amalthea during the outbound trajectory of Pioneer 11.

7.3. *Validation against very energetic observations*

Figure 11 shows the validation of the model against very energetic measurements. Salammbô predicts a depletion of a factor 40 for the >80 MeV fluxes near Io, what cannot be validated by the Pioneer 10 measurements because these are only available inside Io's orbit. Inward of Io, there is a very good match between Salammbô and the Pioneer 10, with or without EMIC waves. Also, the small flux depletion observed during the outbound trajectory near Thebe is correctly reproduced.

Above a distance to the center of Jupiter of 2.3 Rj, our simulations suggest that the channel P1 of Galileo Probe EPI only measures trapped electrons. The proton model correctly reproduces the counts observed there by P2 and P3. Our study of the contamination by alpha particles (see Appendix A) shows that P2 and P3 are very likely to be contaminated between 1.8 and 2.3 Rj, while a different assumption on the response of P1 to alpha particles might lead to the same conclusion for this channel. We therefore consider that the "bump" seen in Galileo Probe EPI proton channels is a contamination by alpha particles. Inside 1.8 Rj, a major discrepancy between Salammbô and the observed counts, of a factor 100 to 1000, is noted. We infer this discrepancy to the main ring, which has been shown to be able to play a major role there in section 4.4 and is not included in the present model.

8. Summary and discussion

A physical model, named Salammbô, of the trapped protons with kinetic energies greater than 1 MeV inside Europa's orbit has been presented. It is the first physics-based model of the proton radiation belts of Jupiter ever proposed, what gives for the first time a tool to not only predict the radiative environment near Jupiter but to also study the physical processes balance in the Jovian proton radiation belts. It relies on an outer boundary condition at L=9.5 provided by the empirical model GIRE3 developed by Garrett et al. (2017) that correctly reproduces the observations used to validate Salammbô.

All physical processes able to shape the proton belts have been introduced, among which is radial diffusion. The assumption on the radial diffusion rate has been validated against >15 MeV observations and Galileo Probe measurements in section 7. We note that the radial diffusion rate used in this study is very similar to what has been proposed by Nénon et al. (2017) for the trapped electrons. As it is generally assumed around Earth and Saturn that the radial diffusion is the same for electrons and protons (Lejosne et al., 2012; Kollmann et al., 2013), the previous note tends to show that the present proton model somewhat validates the radial diffusion rate of the electron model and vice-versa. The adopted radial diffusion coefficient in our physical models is consistent with what has been proposed by Bespalov and Savina (2016), and therefore supports the hypothesis that electric fields in the Io torus might be the origin of the radial transport of radiation belt particles in the inner Jovian magnetosphere. A dependence of the radial diffusion coefficient with kinetic energy might exist, but it would give a rate decreasing with increasing kinetic energies if similar to what is

found around Earth (Lejosne et al., 2013), what goes in the opposite direction of what would be needed in our model to reproduce intense MeV flux drops near Io's orbit with a radial coefficient validated against 15 MeV measurements.

Coulomb collisions with the plasma ions and free electrons of the magnetodisc have been modeled. Our simulations show that, according to the density model of Divine and Garrett (1983), these elastic collisions play a minor role. Charge exchange with the neutral gas torus of Io and Europa has also been shown to be negligible for a model which intends to reproduce >1MeV fluxes, independently of the neutral densities near Io or Europa.

Absorption by the moons clearly plays a major role in the proton belts of Jupiter. Interactions with the Jovian atmosphere, including absorption in the loss cone, Coulomb collisions and charge exchange with atmospheric atoms and particles, also have a predominant effect in our model as they remove field-aligned protons bouncing within or close to the atmosphere.

Equatorial pitch-angle diffusion by 0.4-0.7 Hz EMIC waves have been simulated near Io. As reported in section 4, this frequency range has been assumed to dominate over other frequencies. Our wave-particle simulations have shown that, according to the electron and ion densities given by Bagenal (1994), 0.4-0.7 Hz EMIC waves resonate with 1 MeV low equatorial pitch angle protons and higher energy higher equatorial pitch-angle protons (see Figure 6). The intensity of the waves, or spectral magnetic densities, is only known in the vicinity of Io (see section 4), so that the drift averaged magnetic spectral density has been tuned between 0 and the values measured by the Galileo/MAG experiment. Validations with an adopted value of $2\ nT^2.Hz^{-1}$ have been presented. This demonstrated that scattering by EMIC waves is of major importance since it dominates over moon absorption and charge exchange losses near Io on all kinetic energies above 1 MeV, as was suspected by Thomsen et al. (1977).

Then, the validations presented in section 7 try to explain the flux depletions observed near the orbit of Io. Salammbô tries puts a scientific context on what future equatorial observations might see with the Europa-Clipper and JUICE missions, but does not fully close the following questions: what physical process may sweep near Io equatorial protons in the MeV to tens of MeV range ? What is the origin of the two orders of magnitude flux depletion seen at 1 MeV by Pioneer 10, Pioneer 11, Galileo, and Juno ? Wave-particle interaction with EMIC waves has been proposed in this study but does the magnetic field configuration observed by Galileo in the wake of Io influence the drift trajectory of protons, as it may do for trapped electrons (Thorne et al., 1999) ? If so, is the absorption cross section of Io enhanced or reduced ?

The refinement of the Salammbô equatorial pitch angle grid will enable to feed the Salammbô model with on-going Juno/JEDI observations. In addition, a revisited magnetic field model might change our results in the future, especially very close to the planet where currently available models fail to reproduce the magnetic field observed by Juno (Connerney et al., 2017).

Finally, the Salammbô-proton model is able to predict fluxes anywhere inside L=9.5, making it a powerful tool to assess the Jovian radiation belts environment. It may complement

empirical models, as is done in the hybrid electron JOSE model (Sicard-Piet et al., 2011). The outer boundary condition which is consistent with the GIRE3 model makes GIRE3 and Salammbô easy to plug together, so that a common model might be developed in order to predict the harsh radiative environment Juno, Europa-Clipper and JUICE will be confronted to.

Acknowledgements

The authors are thankful for fruitful discussions with Voyager 1 LECP and Galileo Probe EPI Principle Investigators S. M. Krimigis and L. J. Lanzerotti.

We thank I. Rabadan for discussions on charge exchange cross sections.

We are also thankful to S. M. Brooks, H. Throop and M. Showalter for discussions on the Jovian rings.

The research described in this paper by H. Garrett was carried out at the Jet Propulsion Laboratory, California Institute of Technology, Pasadena, CA, USA under a contract with the National Aeronautics and Space Administration.

Voyager 1 15 minutes averaged LECP count rates can be found on the NASA planetary data system (PDS) website in the volume VG1-J-LECP-4-SUMM-SECTOR-15MIN-V1.1.

Appendix A Galileo Probe Energetic Particle Investigation

Figure A1 is extracted from the thesis of Eckhard Pehlke (Pehlke, 2000) and shows the energy-dependent geometric factors of HE, P1, P2, and P3 in response to impacting electrons, protons and alpha particles.

Energy-dependent geometric factors $G(E)$ of the channels P1, P2, and P3 have been scanned from Figure A1. From there, it is possible to integrate over the distribution function of Salammbô to predict counts (in s^{-1}) by:

$$counts = 2\pi * 2 * \int_0^{+\infty} G(E) * \left[\int_0^{\frac{\pi}{2}} p^2 \, f\left(E, y = \sin\left(\alpha_{eq}\right), L\right) * \sin(\alpha) d\alpha \right] dE$$

With p the proton relativistic momentum, $f(E, y, L)$ the distribution function of Salammbô, α and α_{eq} the local and equatorial pitch angles. The factor 2π comes from the integration over the gyration angle, and the factor 2 from the pitch-angle integral being evaluated between 0 and $\frac{\pi}{2}$ while pitch angle values range from 0 to π.

In order to be able to use the count rates measured by the channel HE to study the contamination by alpha particles in P1, P2, and P3, the geometric factors of Figure A1 should be approximated with step functions. In our study, the response of the HE channel to alpha particles is approximated by a step function starting at 400 MeV with a constant geometric factor of $G(HE) = 3.10^{-2} cm^2.sr$. P1, P2 and P3 have the same minimum kinetic energy of

400 MeV and constant geometric factors of respectively $1\,cm^2.sr$, $10^{-1}cm^2.sr$ and $10^{-1}cm^2.sr$.

Assuming that the four previous EPI channels respond to >400 MeV alpha particles means that we assume that they all respond to the same external omnidirectionnal integral flux of alpha particles. This integral flux can be estimated by:

$$J(>400\ MeV) = 4\pi\ \frac{counts(HE)}{G(HE)}$$

Then, the counts which may be attributed to alpha particles in P1, P2 or P3 (Pi) may be estimated with:

$$counts(Pi) = \frac{G(Pi)}{4\pi} * J(>400\ MeV) = \frac{G(Pi)}{G(HE)} * counts(HE)$$

Figure 11 shows counts which might be attributed, from this method, to alpha particles in the P1, P2 and P3 channels.

Table 1 In-situ proton measurements used in this study to validate the Salammbô model

Mission-Instrument-Channel	Energy range	L-coverage
Pioneer 10-TRD-M3	>80 MeV	3 – 9.5
Pioneer 10-CRT	1.2-2.1 MeV 14.8-21.2 MeV	3 – 9.5
Pioneer 11-CRT	1.2-2.1 MeV 14.8-21.2 MeV	1.4 – 9.5
Pioneer 11 – GTT	0.5 to 3.6 MeV	1.4 – 9.5
Voyager 1 – LECP – PSA3	16.3 to 26.2 MeV	5 – 9.5
Galileo Probe – EPI – P1, P2, P3	See appendix A	1 – 5
Galileo Orbiter – EPD/LEMMS – B0	3.2 to 10.1 MeV	≈ 3 – 9.5
Galileo Orbiter – EPD/CMS – TP3	0.54 to 1.25 MeV	≈ 3 – 9.5

Table 2 Mean excitation energies of oxygen and sulfur neutral atoms and ions.

Atomic particle or ion	Mean excitation energy I_i
O	95.0 eV
O^+	125.2 eV
O^{++}	157.2 eV
S	180 eV
S^+	195.5 eV
S^{++}	232.5 eV
S^{+++}	276.9 eV

Figure 1 Minimum kinetic energy of equatorially mirroring particles simulated by the Salammbô-electron (Nénon et al., 2017) and Salammbô-proton models using a lower kinetic energy boundary of 25 keV at L=9.5.

Figure 2 Trajectories of the Pioneer 10, Pioneer 11, Voyager 1, Galileo Probe, Galileo Orbiter and Juno (only perijove 1) spacecraft in a magnetic dipole frame. The magnetic dipole is set to fit the internal magnetic field model O6 (Connerney et al., 1993).

Figure 3 Absorption cross section of a moon when the proton gyroradius is smaller than the moon radius (left) or bigger than the moon radius (right). Purple circles represent limit trajectories of protons impacting the moon. When the proton gyroradius is bigger than the moon radius, a guiding-center zone within the moon exists where protons would turn around the moon and not be absorbed.

Figure 4 Extensions of the Io and Europa gas torus in a jovigraphic plan, with z along the spin axis of Jupiter.

Figure 5 Charge exchange cross sections of protons on neutral oxygen atoms.

Figure 6 Panel a) Equatorial pitch-angle and kinetic energy diffusion coefficients associated to EMIC waves near Io. Panel b) Absorption and friction coefficients associated to the other physical processes. When a coefficient is not on the plot, it means that its value is under the minimum value of the vertical axis.

Figure 7 Panel a) Omnidirectional integral flux of trapped protons in a magnetic meridian plan. The yellow dashed line shows the Galileo Probe trajectory. The grey area in the >1 MeV plot reminds that Salammbô cannot predict 1 MeV protons inside L=3 (see section 2). Panels b), c) and d) show the kinetic energy spectra of the predicted omnidirectional differential fluxes at the magnetic equator, taking into account or not charge exchange with the Io and Europa gas torus and resonant interactions with EMIC waves near Io. Sharp flux drops at low energies are an artifact.

Figure 8 Validation of the Salammbô model with (in red) or without (in purple) taking into account wave-particle interaction with EMIC waves against 1 to 3 MeV in-situ measurements (in blue). For the Galileo validation, only the prediction at the magnetic equator is shown. Orange areas show the Mc Ilwain parameters intercepted by Io. The grey area shows the Mc Ilwain parameters intercepted by Thebe.

Figure 9 Predictions of the Salammbô model without EMIC waves along the trajectory of Pioneer 10. The purple curve gives the prediction with an assumed maximum density of neutral oxygen near Io of $35\ cm^{-3}$, while the green curve gives the prediction with an unrealistically high maximum density of $3500\ cm^{-3}$.

Figure 10 Validation of the Salammbô model against 15 MeV proton measurements. Orange areas show the Mc Ilwain parameters intercepted by Io, while the grey areas show when Thebe (T), Amalthea (A) and Metis+Adrastea (M+Ad) intercept.

Figure 11 Validation of the Salammbô model against very energetic proton in-situ measurements. Orange areas show the Mc Ilwain parameters intercepted by Io and the grey areas the ones intercepted by Thebe. Note that the Galileo/EPI panels are in counts. The model count rates were calculated by applying the instrument response to the modeled intensities (see Appendix A).

Figure A1 Geometric factors of HE, P1, P2, and P3 channels in response to electrons, protons and alpha particles. Figure reproduced from Pehlke (2000).

References

Bagenal, F., and P. A. Delamere (2011), Flow of mass and energy in the magnetospheres of Jupiter and Saturn, J. Geophys. Res. Space Physics, 116(A5), doi:10.1029/2010ja016294

Bagenal, F., R. J. Wilson, S. Siler, W. R. Paterson, and W. S. Kurth (2016), Survey of Galileo plasma observations in Jupiter's plasma sheet, J. Geophys. Res. Planets, 121, doi:10.1002/2016JE005009

Bagenal, F. (1994), Empirical model of the Io plasma torus: Voyager measurements, J. Geophys. Res. Space Physics, 99(A6), 11043, doi:10.1029/93ja02908

Barnett C.F., H. T. Hunter, M. I. Fitzpatrick, I. Alvarez, C. Cisneros and R. A. Phaneuf (1990), Atomic data for fusion. Volume 1: Collisions of H, H2, He and Li atoms and ions with atoms and molecules, NASA STI/Recon Tech. Rep. N 911, 13238, The Controlled Fusion Atomic Data Center

Bespalov, P. A., and O. N. Savina (2016), Features of the radial diffusion of energetic electrons in the middle Jovian magnetosphere, Cosmic Research, 54(3), 204-208

Beutier, T., D. Boscher, and M. France (1995), Salammbô: A three-dimensional simulation of the proton radiation belt, J. Geophys. Res., 100(A9), 17,181–17,188, doi:10.1029/94JA02728

Bianco-Cano X., C. T. Russell and R. J. Strangeway (2001), The Io-mass loading disk: wave dispersion analysis, J. Geophys. Res. 106 (A11), 26261-26275

Bolton S. J., S. Levin and F. Bagenal (2017), Juno's first glimpse of Jupiter's complexity, Geophys. Res. Lett., doi: 10.1002/2017GL074118

Bourdarie S. A. and V. F. Maget (2012), Electron radiation belt data assimilation with an Ensemble Kalman filter relying on the Salammbô code, Ann. Geophys., 30, 929-943, doi: 10.5194/angeo-30-929-2012

Brice, N., and T. R. Mcdonough (1973), Jupiter's radiation belts, Icarus, 18(2), 206–219, doi:10.1016/0019-1035(73)90204-2

Brooks S. M., L. W. Esposito, M. R. Showalter and H. B. Throop (2004), The size distribution of Jupiter's main ring from Galileo imaging and spectroscopy, Icarus 170 (1), doi: 10.1016/j.icarus.2004.03.003

Burns, J. A. et al. (1999), The Formation of Jupiter's Faint Rings, Science, 284(5417), 1146–1150, doi:10.1126/science.284.5417.1146

Claflin E. S. (1970), Charge-exchange cross sections for hydrogen and helium ions incident on atomic hydrogen: 1 to 1000 keV, Rep. SAMSO-TR-70-258, Space Physics Laboratory, US Air Force, Los Angeles, CA

Connerney et al. (2017), Jupiter's magnetosphere and aurorae observed by the Juno spacecraft during its first polar orbits, Science 356 (6340), 826-832, doi: 10,1126/science.aam5928

Connerney, J. E. P. (1993), Magnetic fields of the outer planets, J. Geophys. Res., 98(E10), 18659, doi:10.1029/93je00980.

Cooper J. F. (1983), Nuclear cascades in Saturn's rings - Cosmic ray albedo neutron decay and origins of trapped protons in the inner magnetosphere, J. Geophys. Res. 88, 3945-3954, doi: 10,1029/JA088iA05p03945

803 Divine, N., and H. B. Garrett (1983), Charged particle distributions in Jupiter's
804 magnetosphere, J. Geophys. Res., 88(A9), 6889-6903, doi:10.1029/JA088iA0909p06889
805 Fillius R. W. and C. E. McIlwain (1974), Measurements of the Jovian radiation belts, J.
806 Geophys. Res. 79 (25)
807 Fillius R. W., A. Mogro-Campero and C. McIlwain (1975), Radiation belts of Jupiter: a
808 second look, Science 188, 465-467
809 Fischer, H., J. Mihalov, L. Lanzerotti, G. Wibberenz, K. Rinnert, F. Gliem, and J. Bach
810 (1992), Energetic Particles Investigation (EPI), Space Science Reviews, 60(1-4),
811 doi:10.1007/bf00216850
812 Fischer H. M., E. Pehlke, G. Wibberbez, L. J. Lanzerotti and J. D. Mihalov (1996), High-
813 energy charged particles in the innermost Jovian magnetosphere, Science 272, 856-858
814 Fujiwara K. (1976), Coulomb-born calculation of charge transfer cross sections of highly-
815 ionized atoms, Journal of the Physical society of Japan, 41 (4)
816 Garrett H., I. Jun, R. Evans, W. Kim and D. Brinza, The latest Jovian trapped proton and
817 heavy ion models, IEE Trans. On Nucl. Science, doi: 10.1109/TNS.2017.2755618
818 Hess W. N. (1959), Van Allen belt protons from Cosmic Ray Neutron Leakage, Phys. Rev., 3,
819 145-145, doi: 10,1103/PhysRevLett.3.145.4
820 Horne R. B., N. P. Meredith, S. A. Glauert and T. Kersten (2016), Wave-driven diffusion in
821 radiation belt dynamics, In waves, particles and storms in geospace, edited by G. Balasis, I. A.
822 Daglis and I. R. Mann, Oxford University press
823 Jensen P. W. K., S. P. A. Sauer, J. Oddershede and J. R. Sabin (2016), Mean excitation
824 energies for molecular ions, Nuc. Inst. And Methods in Phys. Res. B, 394, 73-80, doi:
825 10.1016/j.nimb.2016.12.034
826 Jun, I., J. M. Ratliff, H. B. Garrett, and R. W. McEntire (2002), Monte Carlo simulations of
827 the Galileo energetic particle detector, Nuclear Instruments and Methods in Physics Research
828 Section A: Accelerators, Spectrometers, Detectors and Associated Equipment, 490(3), 465–
829 475, doi:10.1016/s0168-9002(02)01072-0
830 Kennel C. F. and F. Engelmann (1966), Velocity space diffusion from weak plasma
831 turbulence in a magnetic field, Phys. Fluids, 9(12), 2377, doi: 10.1063/1.1761629
832 Kennel C. F. and H. E. Petschek (1966), Limit on stably trapped particle fluxes, J. Geophys.
833 Res. 71, doi: 10.1029/JZ071i001p00001
834 Khurana, K. K. (1997), Euler potential models of Jupiter's magnetospheric field, J. Geophys.
835 Res., 102(6), 11-295, doi:10.1029/97JA00563
836 Kita, H.,H.Misawa, A. Bhardwaj, F. Tsuchiya, T. Sakanoi,Y.Kasaba, C. Tao, Y. Miyoshi, and
837 A. Morioka (2015), Relation between the short-term variation of the Jovian radiation belt and
838 thermosphere derived from radio and infrared observations, J. Geophys. Res. Space Physics,
839 120, 6614–6623, doi:10.1002/2015JA021374
840 Kivelson M. G. et al. (1996), Io's interaction with the plasma torus: magnetometer report,
841 Science, 274 (5286), 396-398, doi: 10.1126/science.274.5286.396
842 Koller J., Y. Chen, G. D. Reeves, R. H. W. Friedel, T. E. Cayton and J. A. Vrugt, Identifying
843 the radiation belt source region by data assimilation, J. Geophys. Res. Space Physics 112
844 (A6), doi: 10.1029/2006JA012196

Kollmann P. E., E. Roussos, C. Paranicas, N. Krupp and D. J. Haggerty (2013), Processes forming and sustaining Saturn's proton radiation belts, Icarus, 222, 323-341, doi: 10.1016/j.icarus.2012.10.033

Kollmann P., E. Roussos, A. Kotova, J. F. Cooper, D. G. Mitchell, N. Krupp and C. Paranicas (2015), MeV proton flux predictions near Saturn's D ring, J. Geophys. Res. Space Physics 120 (10), doi: 10.1002/2015JA021621

Kollmann P., C. Paranicas, G. Clark, E. Roussos, A. Lagg and N. Krupp (2016), The vertical thickness of Jupiter's Europa torus from charged particle measurements, Geophys. Res. Lett. 43 (18), doi: 10.1002/2016GL070326

Kollmann P. et al. (2017), A heavy ion and proton radiation belt inside of Jupiter's rings, Geophys. Res. Lett. 44 (11), 5259-5268, doi: 10.1002/2017GL073730

Krimigis S. M. and T. P. Armstrong (1982), Two-component proton spectra in the inner Saturnian magnetosphere, Geophys. Res. Lett., 9, 1143-1146, doi: 10.1029/GL009i010p01143

Krimigis S. M., C. O. Bostrom, T. P. Armstrong, W. I. Axford, C. Y. Fan, G. Gloeckler and L. J. Lanzerotti (1977), The Low Energy Charged Particle experiment on the Voyager spacecraft, Space Science Reviews 21, doi: 10.1007/BF00211545

Lagg, A., N. Krupp, J. Woch, S. Livi, B. Wilken, and D. J. Williams (1998), Determination of the neutral number density in the Io torus from Galileo-EPD measurements, Geophys. Res. Lett., 25(21), 4039–4042, doi:10.1029/1998gl900070

Lejosne S., D. Boscher, V. Maget and G. Rolland (2012), Bounce-averaged approach to radial diffusion modeling: from a new derivation of the instantaneous rate of change of the third adiabatic invariant to the characterization of the radial diffusion process, J. Geophys. Res.: Space Physics 117 (A8), doi: 10.1029/2012JA018011

Lejosne S., D. Boscher, V. Maget and G. Rolland (2013), Deriving electromagnetic radial diffusion coefficients of radiation belt equatorial particles for different levels of magnetic activity based on magnetic field measurements at geostationary orbit, J. Geophys. Res. Space Physics 118 (6), doi: 10.1002/J. Geophys. Res.a.50361

Lin et al. (1993), ULF waves in the Io torus: Ulysses observations, J. Geophys. Res. 98 (A12), 21151-21162, doi: 10.1029/93JA02593

Lindsay B. G. and R. F. Stebbings (2005), Charge transfer cross sections for energetic neutral atom data analysis, J. Geophys. Res. 110 (A12213), doi: 10.1029/2005JA011298

Lorenzato L., A. Sicard-Piet and S. Bourdarie (2012), A physical model for electron radiation belts of Saturn, J. Geophys. Res. Space Physics 117 (A8), doi: 10.1029/2012JA017560

Mauk B. H. and N. J. Fox (2010), Electron radiation belts of the Solar system, J. Geophys. Res. 115 (A12220), doi: 10.1029/2010JA015660

Mauk B. H. et al. (1998), Galileo-measured depletion of near-Io hot ring current plasmas since the Voyager epoch, J. Geophys. Res. 103, doi: 10.1029/97JA02343

Mauk B. H. et al. (2004), Energetic ion characteristics and neutral gas interactions in Jupiter's magnetosphere, J. Geophys. Res. 109 (A09S12), doi: 10,1029/2003JA010270

Mauk B. H. et al. (2013), The Jupiter Energetic Particle Detector Instrument (JEDI) investigation for the Juno mission, Space Science Review, doi: 10.1007/s11214-013-0025-3

887 Mauk B. H. (2014), Comparative investigation of the energetic ion spectra comprising the
888 magnetospheric ring currents of the Solar system, J. Geophys. Res.: Space Physics, 119, doi:
889 10.1002/2014JA020392
890 Menietti J. D., T. F. Averkamp, S. Y. Ye, R. B. Horne, E. E. Woodfield, Y. Y. Shprits, D. A.
891 Gurnett, A. M. Persoon and J. E. Wahlund (2015), Survey of Saturn Z-mode emission, J.
892 Geophys. Res.: Space Physics 120 (8), doi: 10.1002/2015JA021426
893 Miyoshi, Y., H. Misawa, A. Morioka, T. Kondo, Y. Koyama, and J. Nakajima (1999),
894 Observation of short-term variation of Jupiter's synchrotron radiation, Geophys. Res. Lett.,
895 26, 9–12, doi:10.1029/1998GL900244.
896 Murakami, G., et al. (2016), Response of Jupiter's inner magnetosphere to the solar wind
897 derived from extreme ultraviolet monitoring of the Io plasma torus, Geophys. Res. Lett., 43,
898 12,308–12,316, doi:10.1002/2016GL071675.
899 Nénon Q., A. Sicard and S. Bourdarie (2017), A new physical model of the electron radiation
900 belts of Jupiter inside Europa's orbit, J. Geophys. Res. 122 (5), doi: 10.1002/2017JA023893
901 Paonessa M. and A. F. Cheng (1985), A theory of satellite sweeping, J. Geophys. Res. 90,
902 doi: 10.1029/JA090iA04p03428
903 Pehlke E. (2000), Teilchenpopulationen in der inneren Jupitermagnetosphäre. Untersuchung
904 der EPI-daten von der Galileo Probe, PhD thesis
905 Russell C. T., Y. L. Wang, X. Bianco-Cano and R. J. Strangeway (2001), The Io mass-loading
906 disk: constraints provided by ion cyclotron wave observations, J. Geophys. Res. 106 (A11),
907 26233-26242, doi: 10.1029/2001JA900029
908 Santos-Costa D. and S. Bourdarie (2001), Modeling the inner Jovian electron radiation belt
909 including non-equatorial particles, Planet. Space Sci., 49(3-4), 303-312, doi:10.1016/s0032-
910 0633(00)00151-3
911 Santos-Costa D., M. Blanc, S. Maurice and S. J. Bolton (2003), Modeling the proton and
912 electron radiation belts of Saturn, Geophys. Res. Lett. 30 (20), doi: 10.1029/2003GL017972
913 Santos-Costa, D., and S. J. Bolton (2008), Discussing the processes constraining the Jovian
914 synchrotron radio emission's features, Planetary and Space Science, 56(3-4), 326–345,
915 doi:10.1016/j.pss.2007.09.008
916 Santos-Costa, D., S. J. Bolton, R. M. Thorne, Y. Miyoshi, and S. M. Levin (2008),
917 Investigating the origins of the Jovian decimetric emission's variability, J. Geophys. Res.
918 Space Physics, 113(A1), doi:10.1029/2007ja012396.
919 Sauer S. P. A., J. Oddershede and J. R. Sabin (2015), 'The mean excitation energy of atomic
920 ions', Advances in Quantum chemistry, 71, doi: 10.1016/bs.aiq.2015.02.001
921 Schulz M. and L. J. Lanzerotti (1974), Particle Diffusion in the Radiation Belts, Springer,
922 Berlin
923 Selesnick R. S., A. C. Cummings and B. T. Kress (2013), Direct observation of the CRAND
924 proton radiation belt source, J. Geophys. Res. 118, 7532-7537, doi: 10.1002/2013JA019338
925 Shprits Y., D. Kondrashov, Y. Chen, R. Thorne, M. Ghil, R. Friedel and G. Reeves (2007),
926 Reanalysis of relativistic radiation belt electron fluxes using CRRES satellite data, a radial
927 diffusion model and a Kalman filter, J. Geophys. Res. Space Physics 112 (A12), doi:
928 10.1029/2007JA012579
929 Sicard A. and S. Bourdarie (2001), Physical electron model from Jupiter's surface to the orbit
930 of Europa, J. Geophys. Res. 109 (A02216), doi: 10.1029/2003JA010203

931 Sicard-Piet A., S. Bourdarie, and N. Krupp (2011), JOSE: A new Jovian specification
932 environment model, IEEE Trans. Nucl. Sci., 58(3), 923-931, doi:10.1109/TNS.2010.2097276
933 Sicard-Piet, A., D. Boscher, R. B. Horne, N. P. Meredith, and V. Maget (2014), Effect of
934 plasma density on diffusion rates due to wave particle interactions with chorus and
935 plasmaspheric hiss: extreme event analysis, Annales Geophysicae, 32(8), 1059–1071,
936 doi:10.5194/angeo-32-1059-2014
937 Simpson J. A., D. Hamilton, G. Lentz, R. B. McKibben, A. Mogro-Campero, M. Perkins, K.
938 R. Pyle, A. J. Tuzzolino and J. J. O'Gallagher (1974), Protons and electrons in Jupiter's
939 magnetosphere field: results from the University of Chicago experiment on Pioneer 10,
940 Science 183, 306-309, doi: 10.1126/science.183.4122.306
941 Simpson et al. (1975), Jupiter revisited: first results from the University of Chicago charged
942 particle experiment on Pioneer 11, Science 188, 455-459, doi: 10.1126/science.188.4187.455
943 Smyth W. H. and M. L. Marconi (2006), Europa's atmosphere, gas tori, and magnetospheric
944 implications, Icarus 181, 510-526, doi: 10.1016/j.icarus.2005.10.019
945 Sparks W. B., K. P. Hand, M. A. McGrath, E. Bergeron, M. Cracraft and S. E. Deustua
946 (2016), Probing for evidence of plumes on Europa with HST/STIS, The Astrophysical
947 Journal, 829 (2), doi: 10.3847:0004-637X/829/2/121
948 Störmer C. (1955), The polar aurora, Clarendon Press, Oxford
949 Thomas J. and W. R. Doherty (1972), Calculations of neutron decay proton trapping in the
950 Jovian magnetosphere, Proceedings of the Jupiter radiation belt workshop, JPL technical
951 memorandum 33-543
952 Thomsen M. F., C. K. Goertz and J. A. Van Allen (1977), On determining magnetospheric
953 diffusion coefficients from the observed effects of Jupiter's satellite Io, J. Geophys. Res. 82
954 (35), doi: 10.1029/JA08i035p05541
955 Thorne, R. M., D. J. Williams, L. D. Zhang, and S. Stone (1999), Energetic electron butterfly
956 distributions near Io, J. Geophys. Res. Space Physics, 104(A7), 14755–14766,
957 doi:10.1029/1999ja900132
958 Trainor J. H., F. B. McDonald, B. J. Teegarden, W. R. Webber and E. C. Roelof (1974),
959 Energetic particles in the Jovian magnetosphere, J. Geophys. Res. 79 (25), doi:
960 10.1029/JA079i025p03600
961 Trainor J. H., F. B. McDonald, D. E. Stillwell, B. J. Teegarden and W. R. Webber (1975),
962 Jovian protons and electrons - Pioneer 11, Science 188, 462-465, doi:
963 10.1126/science.188.4187.462
964 Tsuchiya, F., H. Misawa, K. Imai, and A. Morioka (2011), Short-term changes in Jupiter's
965 synchrotron radiation at 325 MHz: Enhanced radial diffusion in Jupiter's radiation belt driven
966 by solar UV/EUV heating, J. Geophys. Res., 116, A09202, doi:10.1029/2010JA016303.
967 Van Allen J. A., B. A. Randall, D. B. Baker, C. K. Goertz, D. D. Sentman, M. F. Thomsen
968 and H. R. Flindt (1975), Pioneer 11 observations of energetic particles in the Jovian
969 magnetosphere, Science 188, 459-462, doi:10.1126/science.188.4187.459
970 Varghese S. L., G. Bissinger, J. M. Joyce and R. Laubert (1985), Atomic total electron-
971 capture cross sections from C-,O-,F- and S-bearing molecular gases for MeV/u H+ and He+
972 projectiles, Physical Review A, 31 (4), doi: 10.1103/PhysRevA.31.2202

Figure 1.

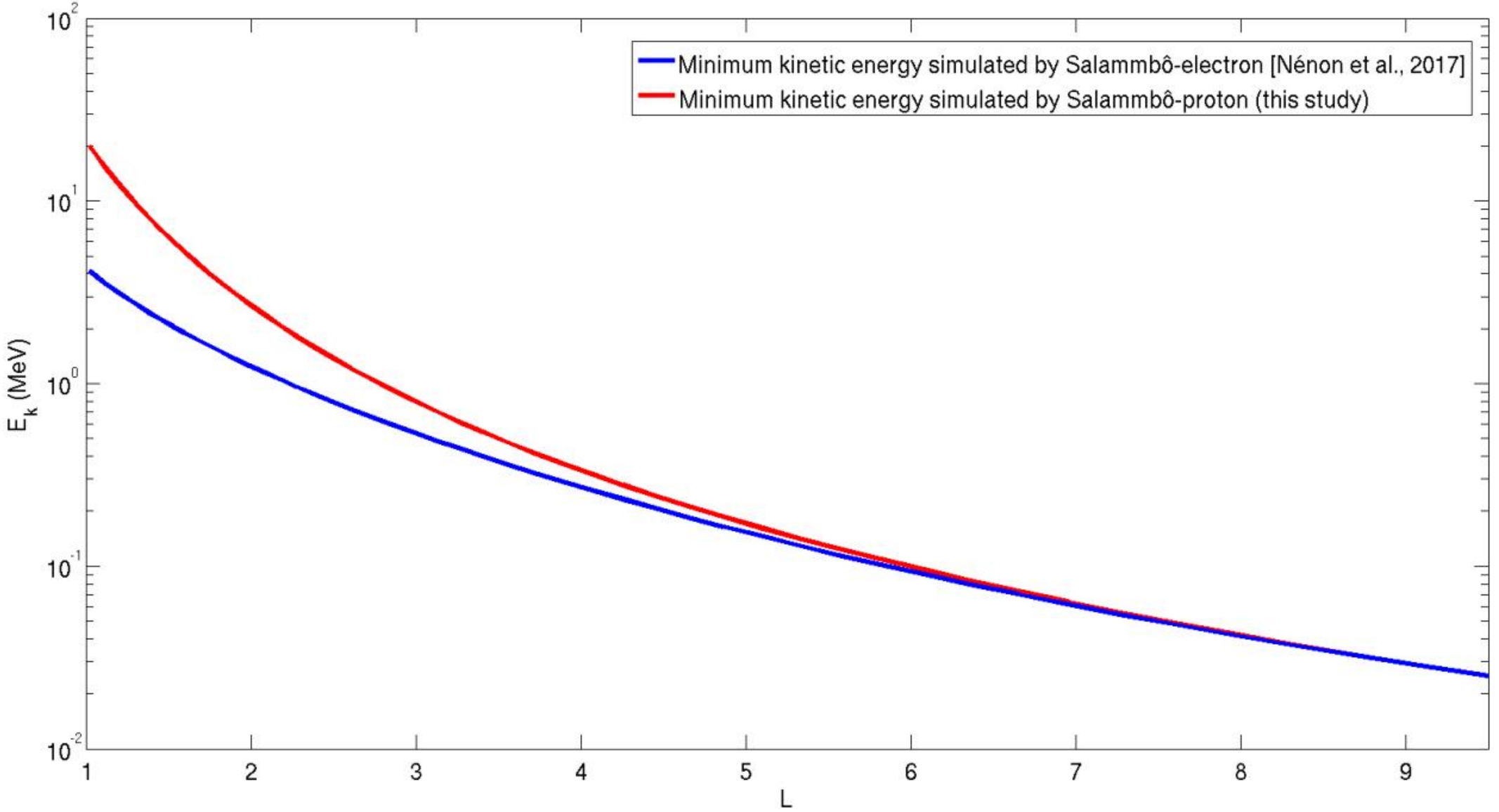
Minimum kinetic energy simulated by Salammbô-electron [Nénon et al., 2017]
Minimum kinetic energy simulated by Salammbô-proton (this study)
10^{2}
10^{1}
10^{0}
10^{-1}
10^{-2}
E_k (MeV)
1
2
3
4
5
6
7
8
9
L

Figure 2.

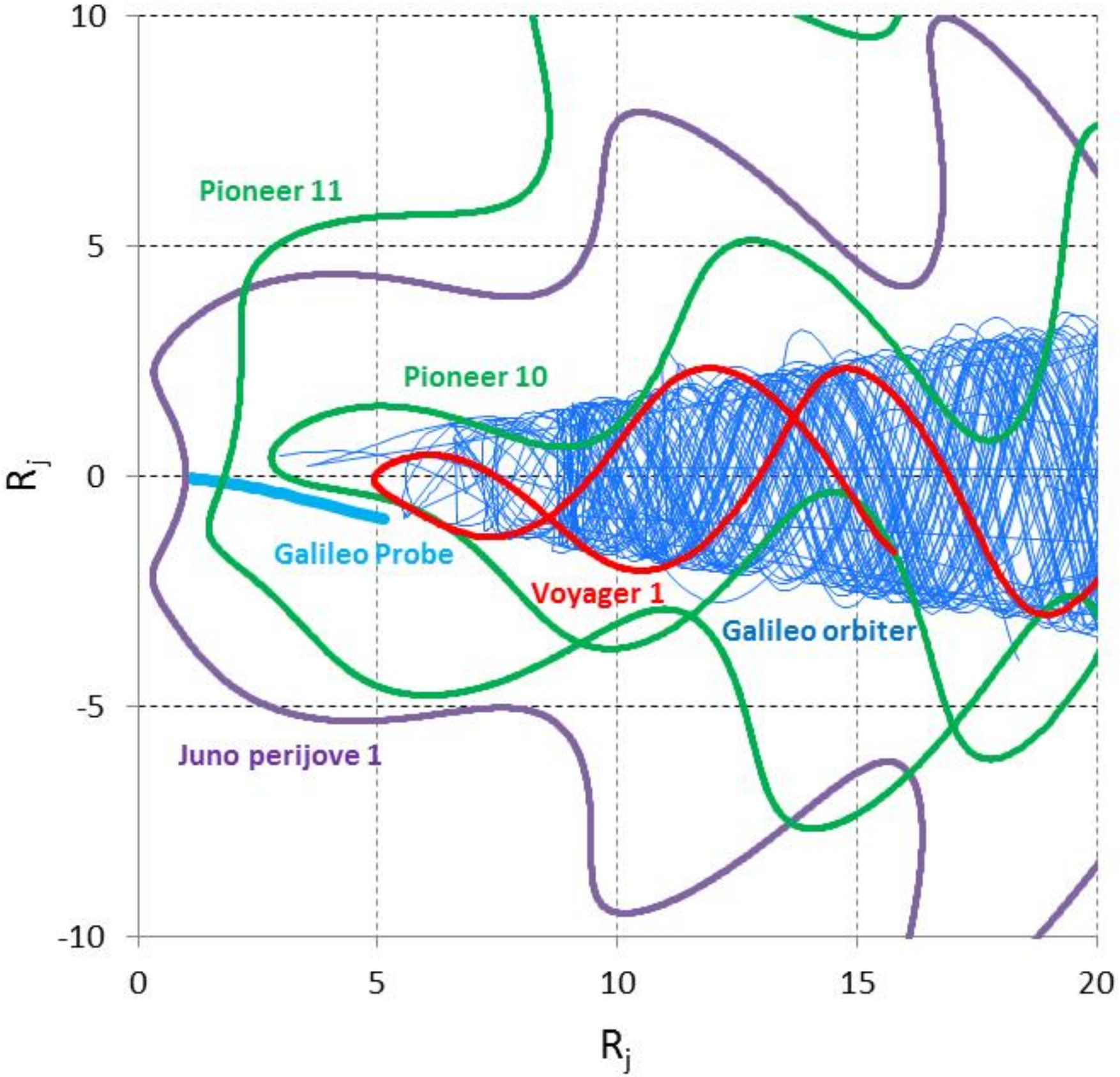
10
5
0
-5
-10
R_j
0
5
10
15
20
R_j
Pioneer 11
Pioneer 10
Galileo Probe
Voyager 1
Galileo orbiter
Juno perijove 1

Figure 3.

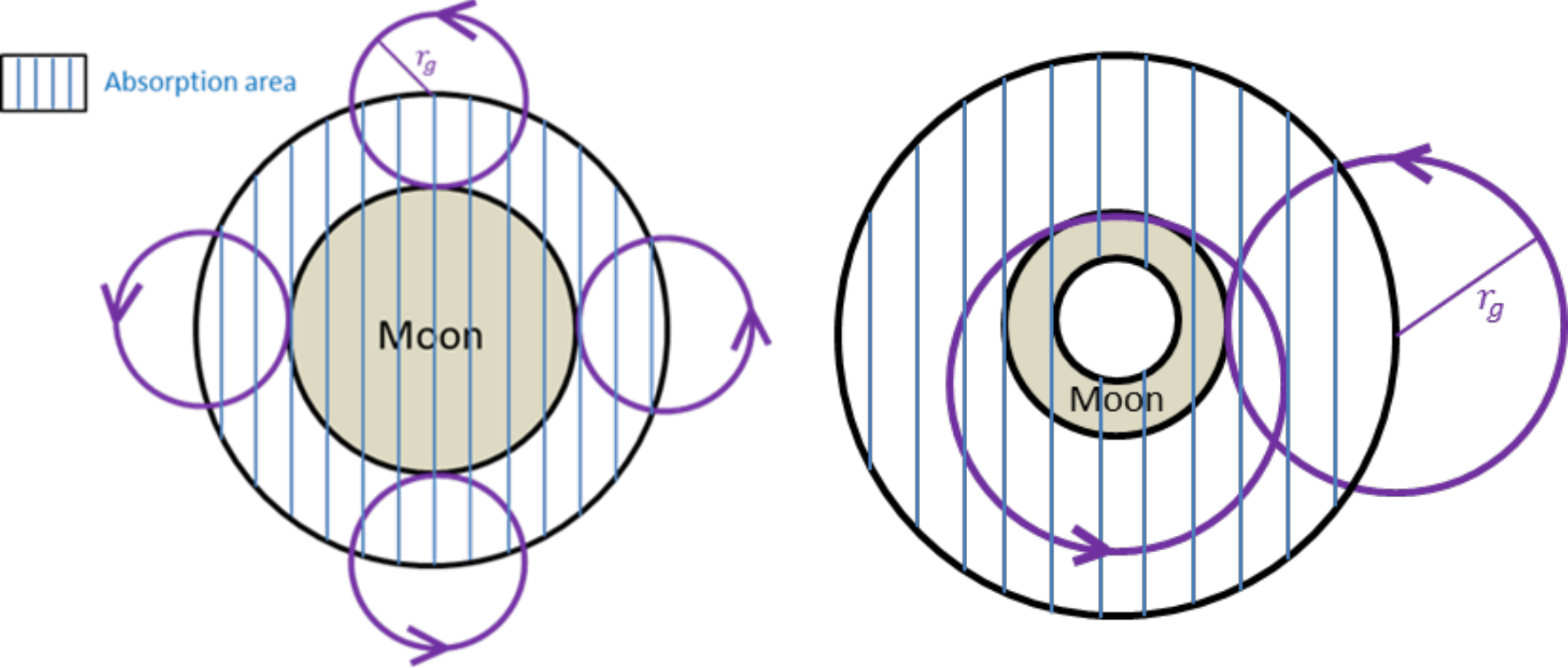
Absorption area
r_g
Moon
Moon
r_g

Figure 4.

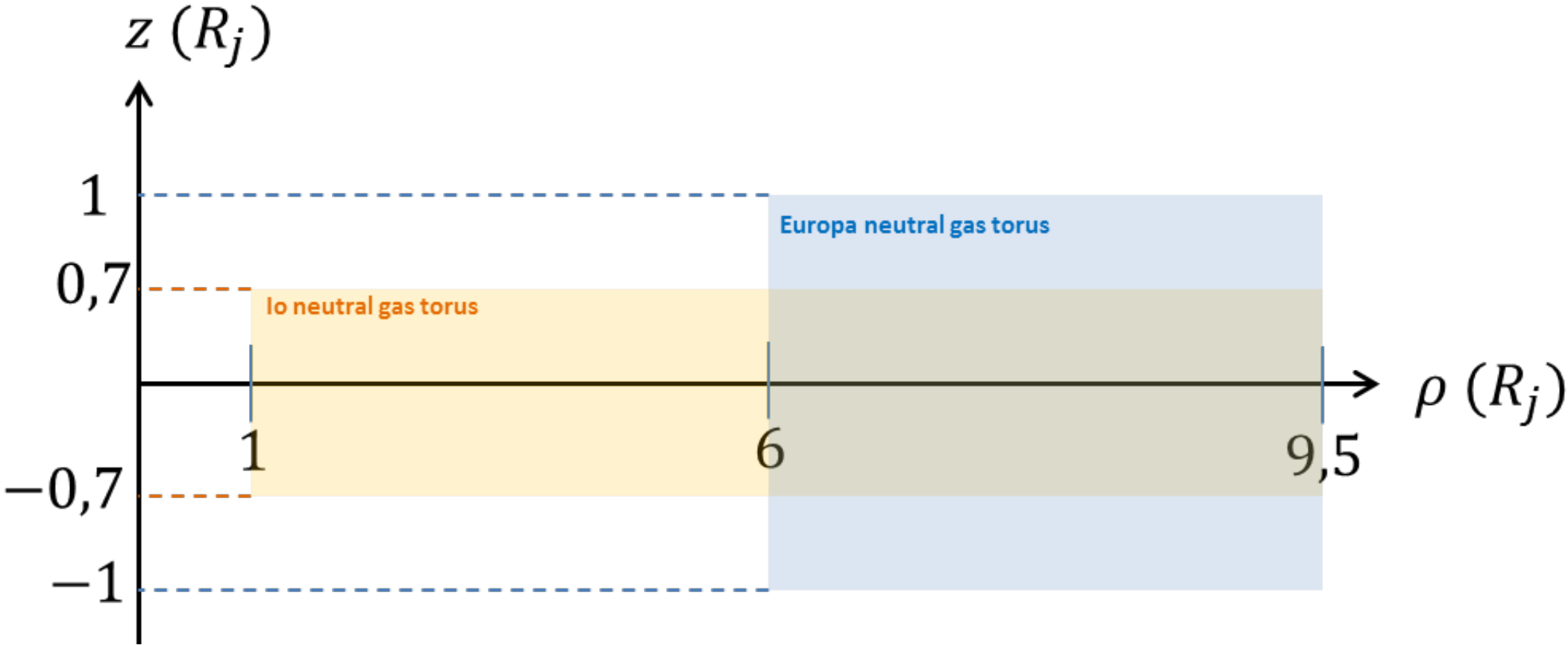
$z\ (R_j)$
1
0,7
$-0,7$
-1
Europa neutral gas torus
Io neutral gas torus
1
6
9,5
$\rho\ (R_j)$

Figure 5.

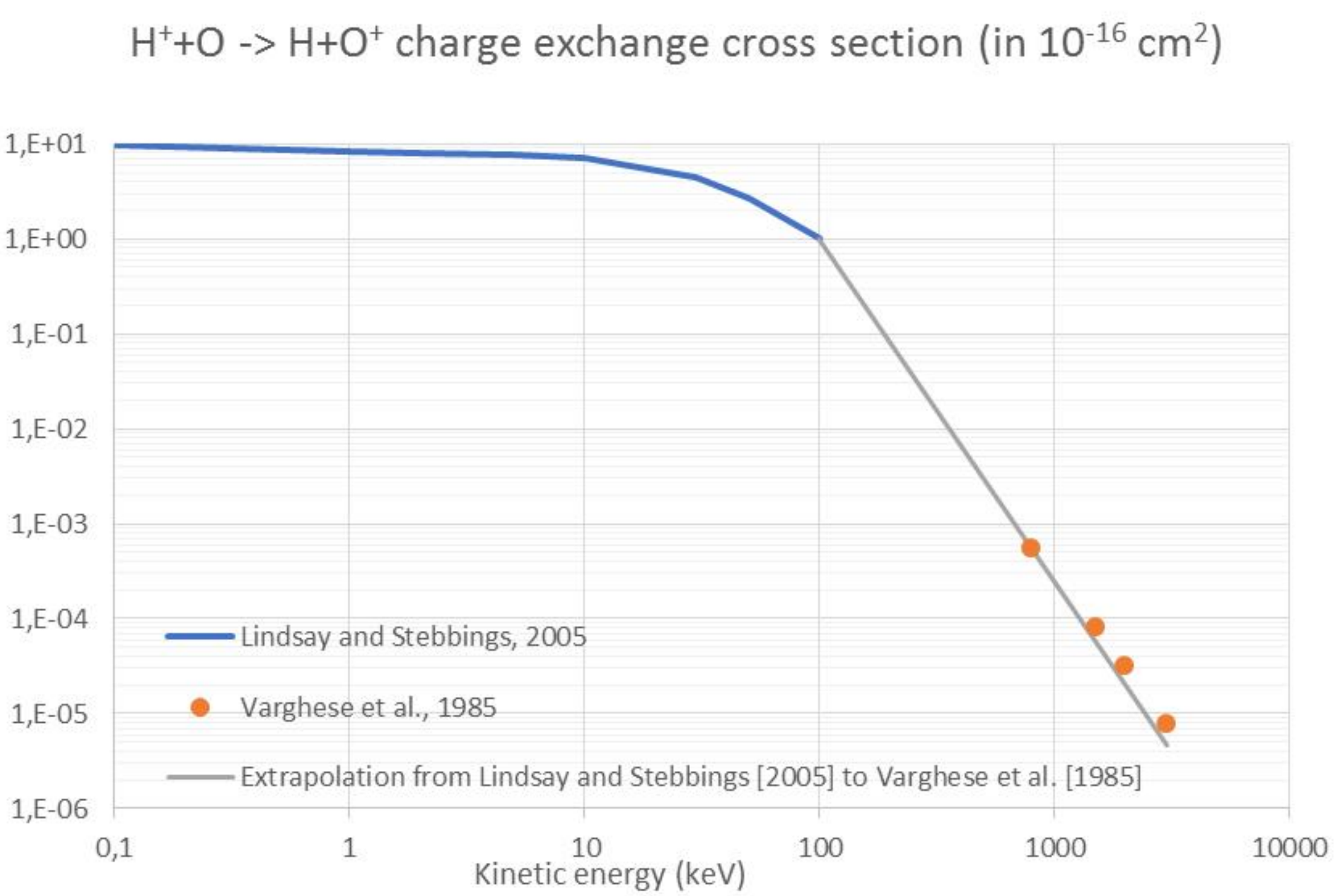
H+ +O -> H+O+ charge exchange cross section (in 10-16 cm2)
1,E+01
1,E+00
1,E-01
1,E-02
1,E-03
1,E-04
1,E-05
1,E-06
0,1
1
10
100
1000
10000
Kinetic energy (keV)
Lindsay and Stebbings, 2005
Varghese et al., 1985
Extrapolation from Lindsay and Stebbings [2005] to Varghese et al. [1985]

Figure 6.

a)

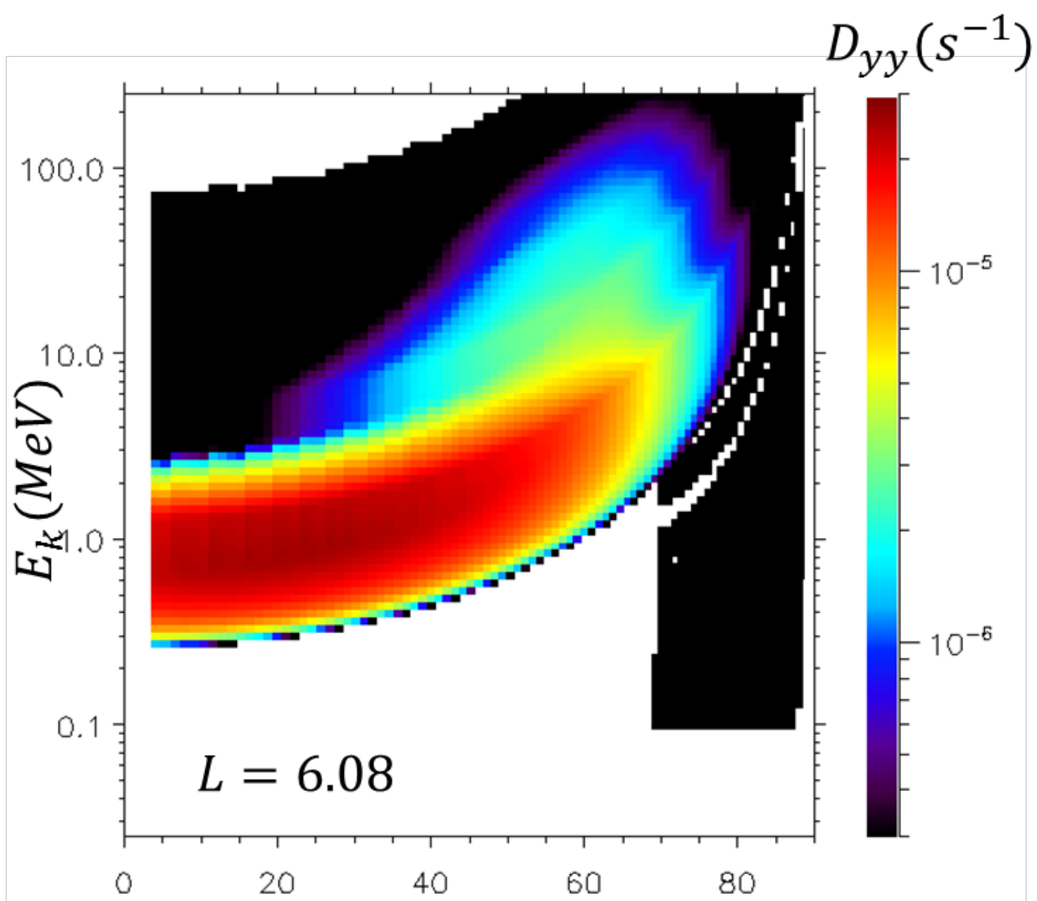

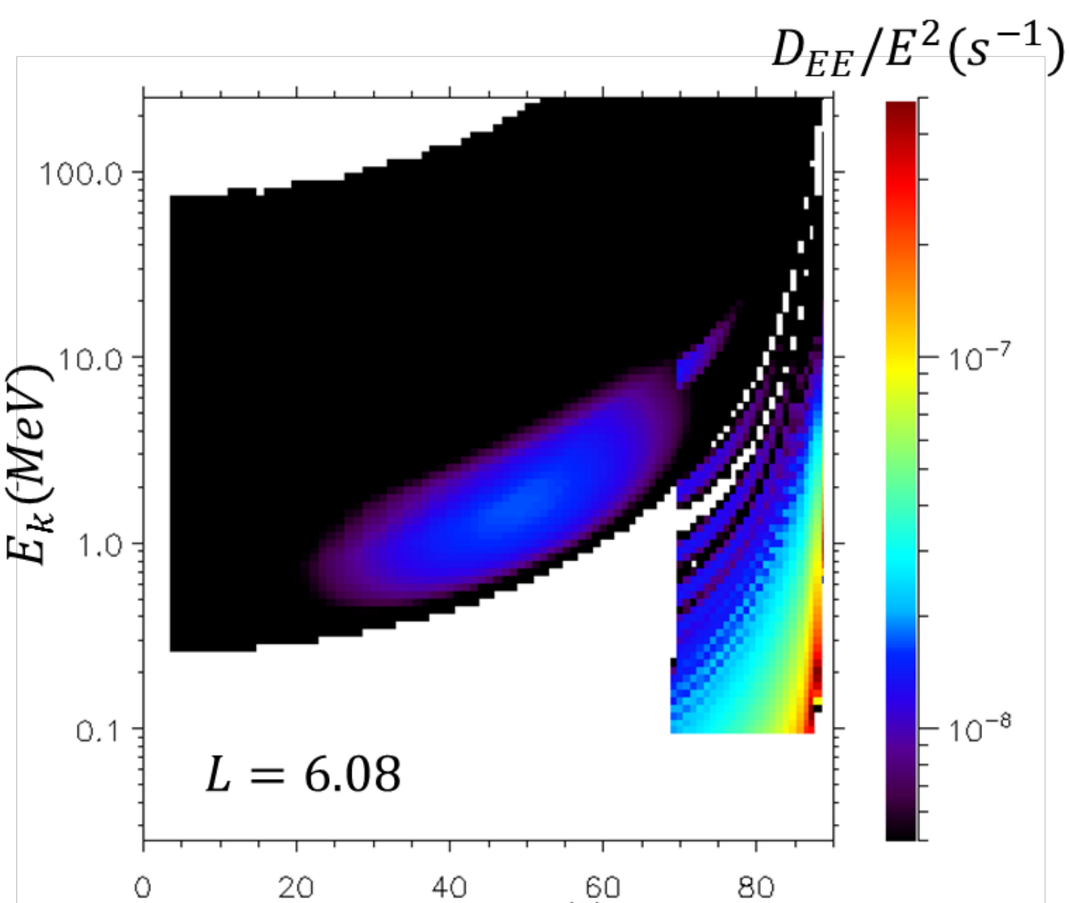

b)

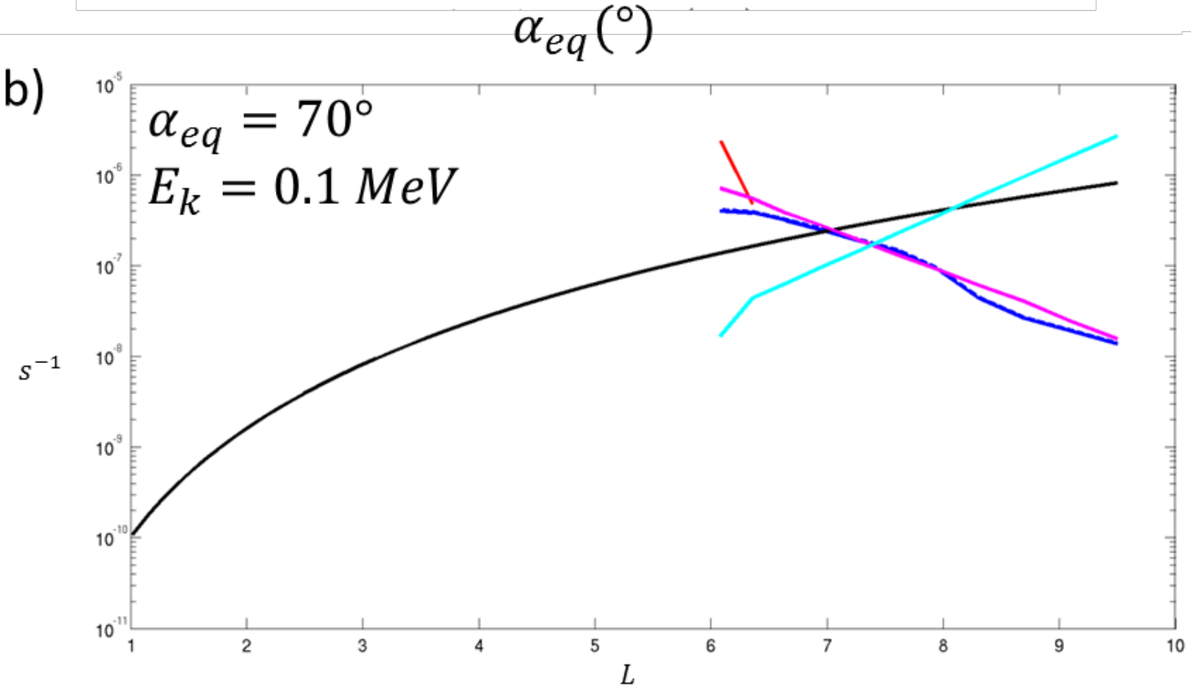

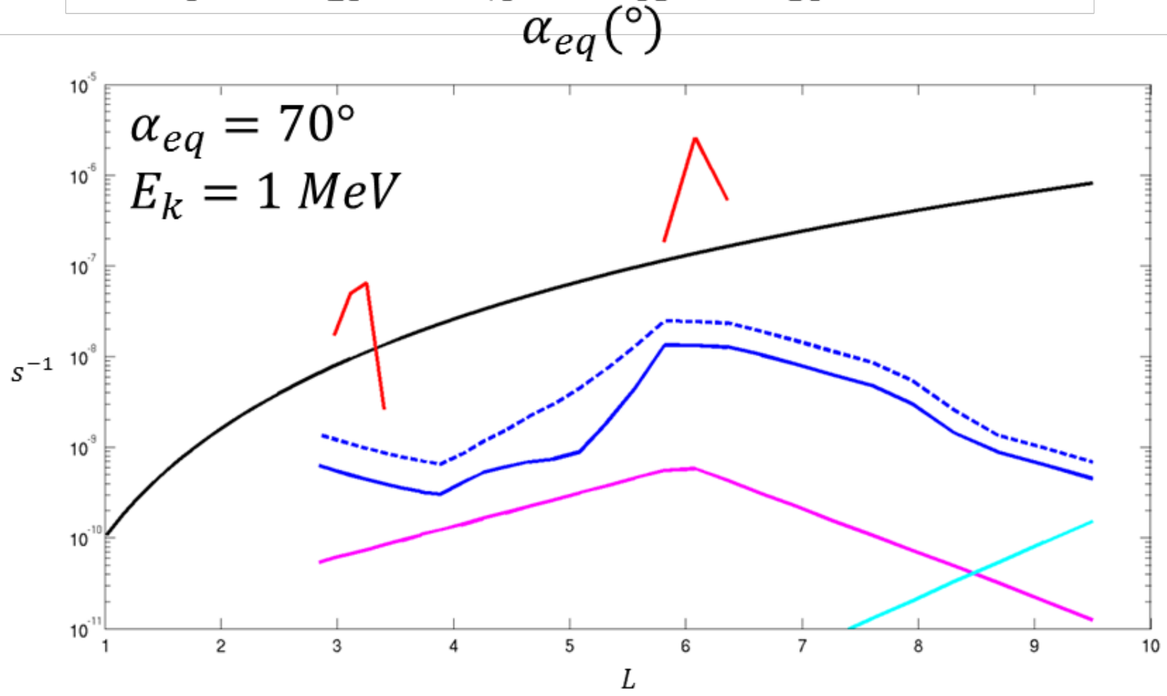

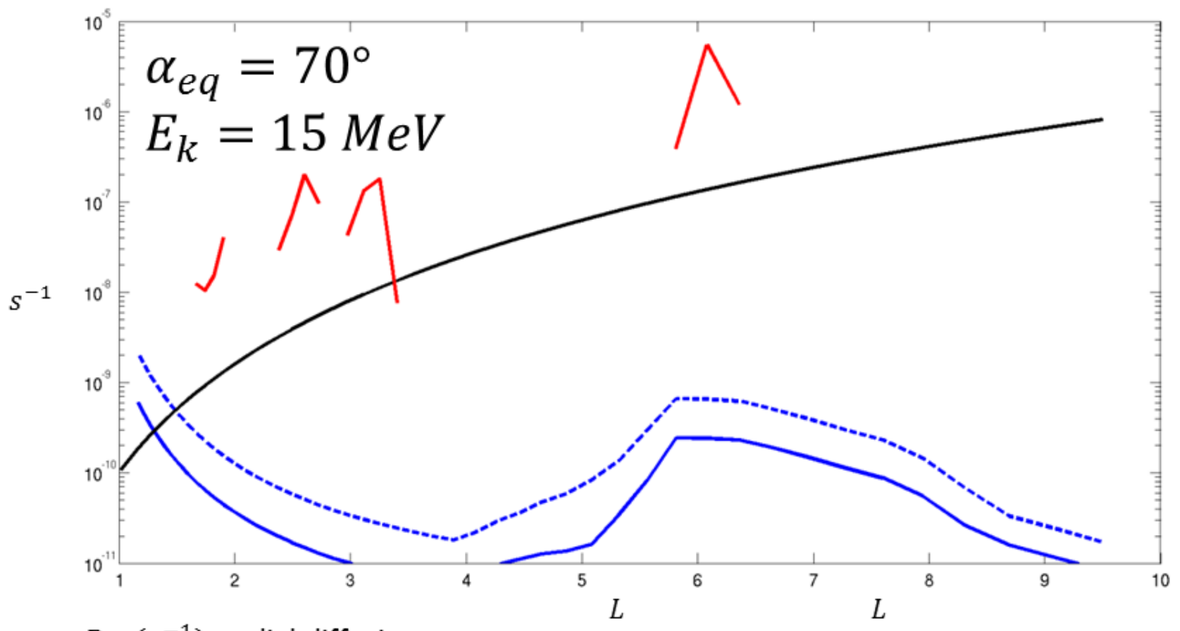

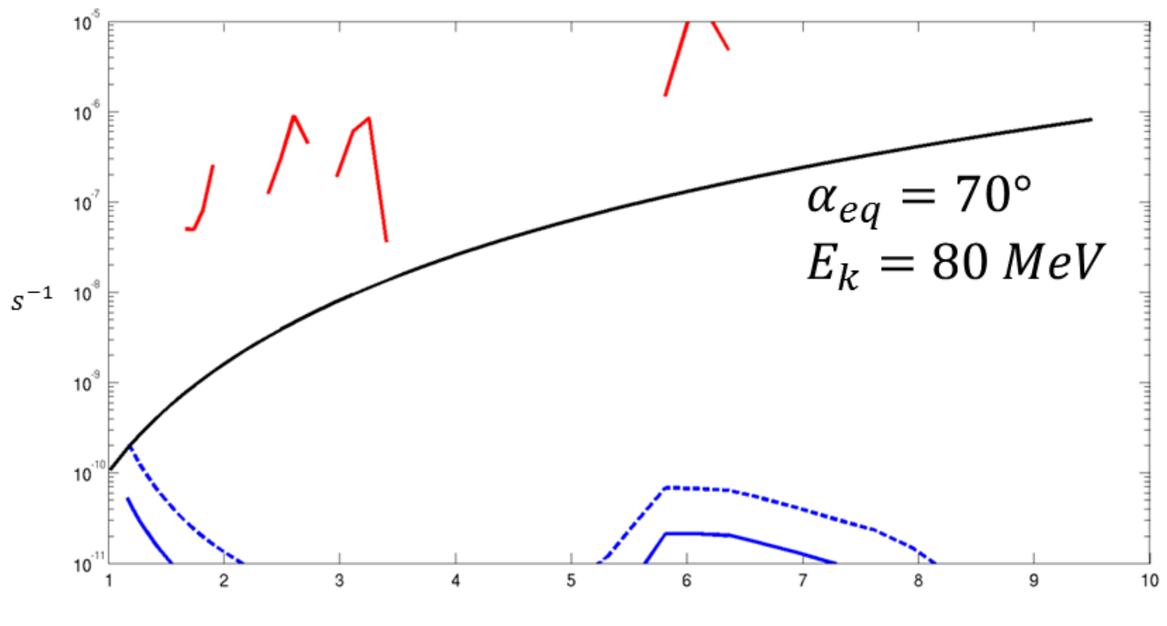

$D_{LL}(s^{-1})$: radial diffusion

$\frac{1}{\Gamma}$ (s^{-1}): absorption by the moons

$\frac{1}{\Gamma}$ (s^{-1}): charge exchange with the Europa gas torus, assuming a maximum neutral density of $410\ cm^{-3}$

$\frac{1}{\Gamma}$ (s^{-1}): charge exchange with the Io gas torus, assuming a maximum neutral density of $35\ cm^{-3}$

$\frac{1}{E_k}\frac{dE_k}{dt}$ (s^{-1}): kinetic energy frictions due to Coulomb collisions neglecting the elastic collisions with the ions of the magnetodisc

$\frac{1}{E_k}\frac{dE_k}{dt}$ (s^{-1}): kinetic energy frictions due to Coulomb collisions taking into account the elastic collisions with the ions of the magnetodisc

Figure 7.

a)

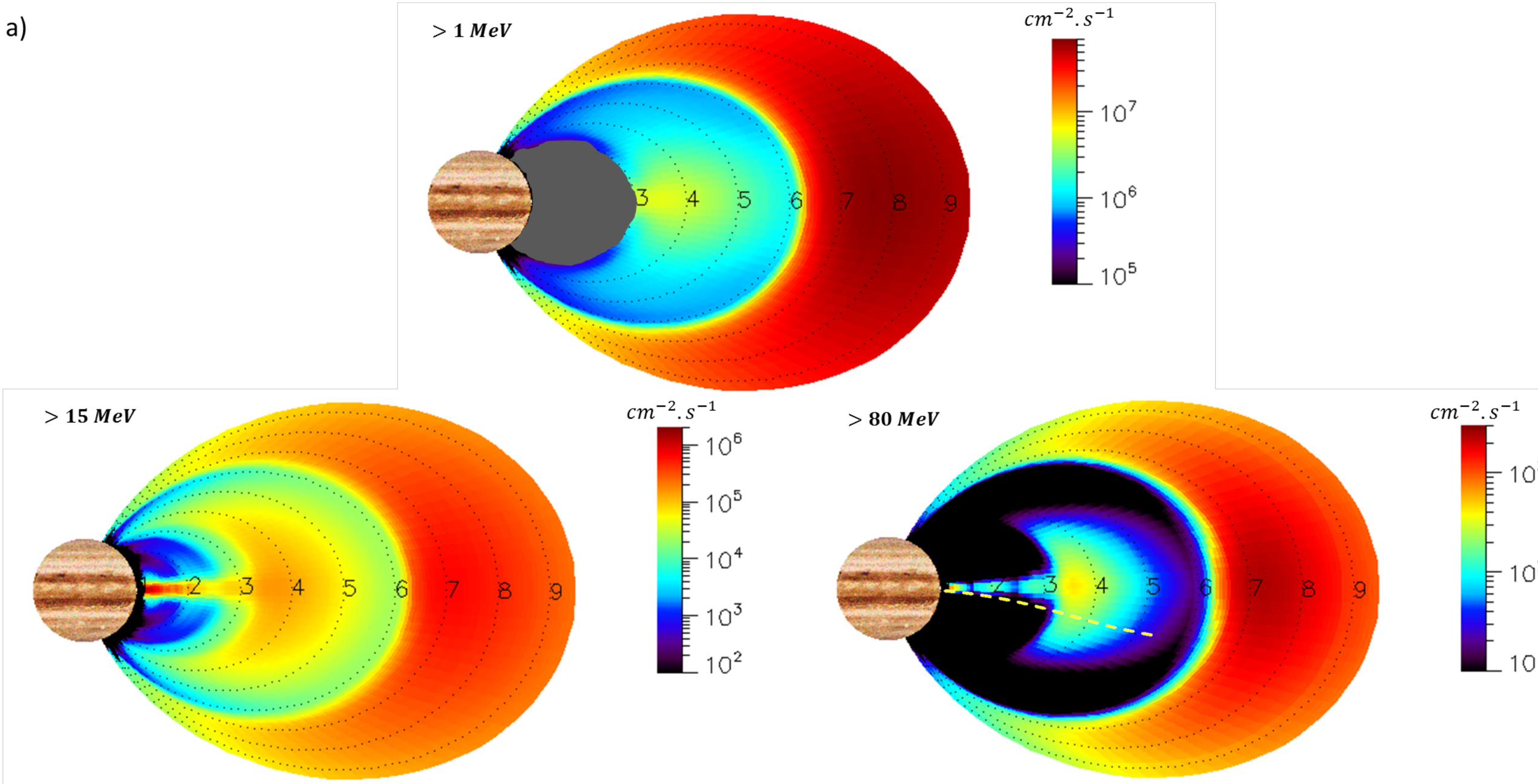
> 1 MeV
cm⁻².s⁻¹
10⁷
10⁶
10⁵
1
2
3
4
5
6
7
8
9
> 15 MeV
cm⁻².s⁻¹
10⁶
10⁵
10⁴
10³
10²
> 80 MeV
cm⁻².s⁻¹
10³
10²
10¹

b)

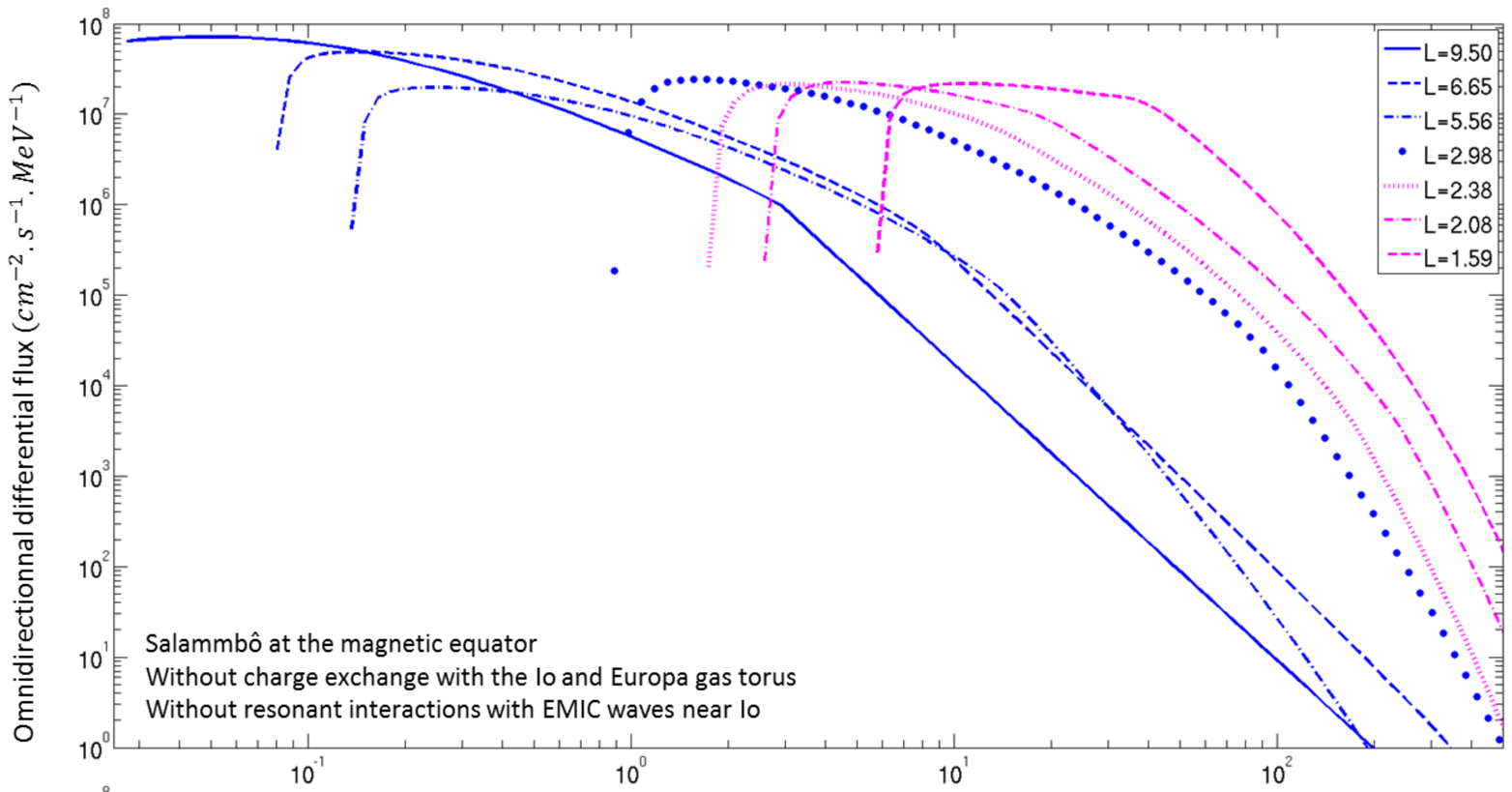
Omnidirectionnal differential flux (cm⁻².s⁻¹.MeV⁻¹)
L=9.50
L=6.65
L=5.56
L=2.98
L=2.38
L=2.08
L=1.59
Salammbô at the magnetic equator
Without charge exchange with the Io and Europa gas torus
Without resonant interactions with EMIC waves near Io

c)

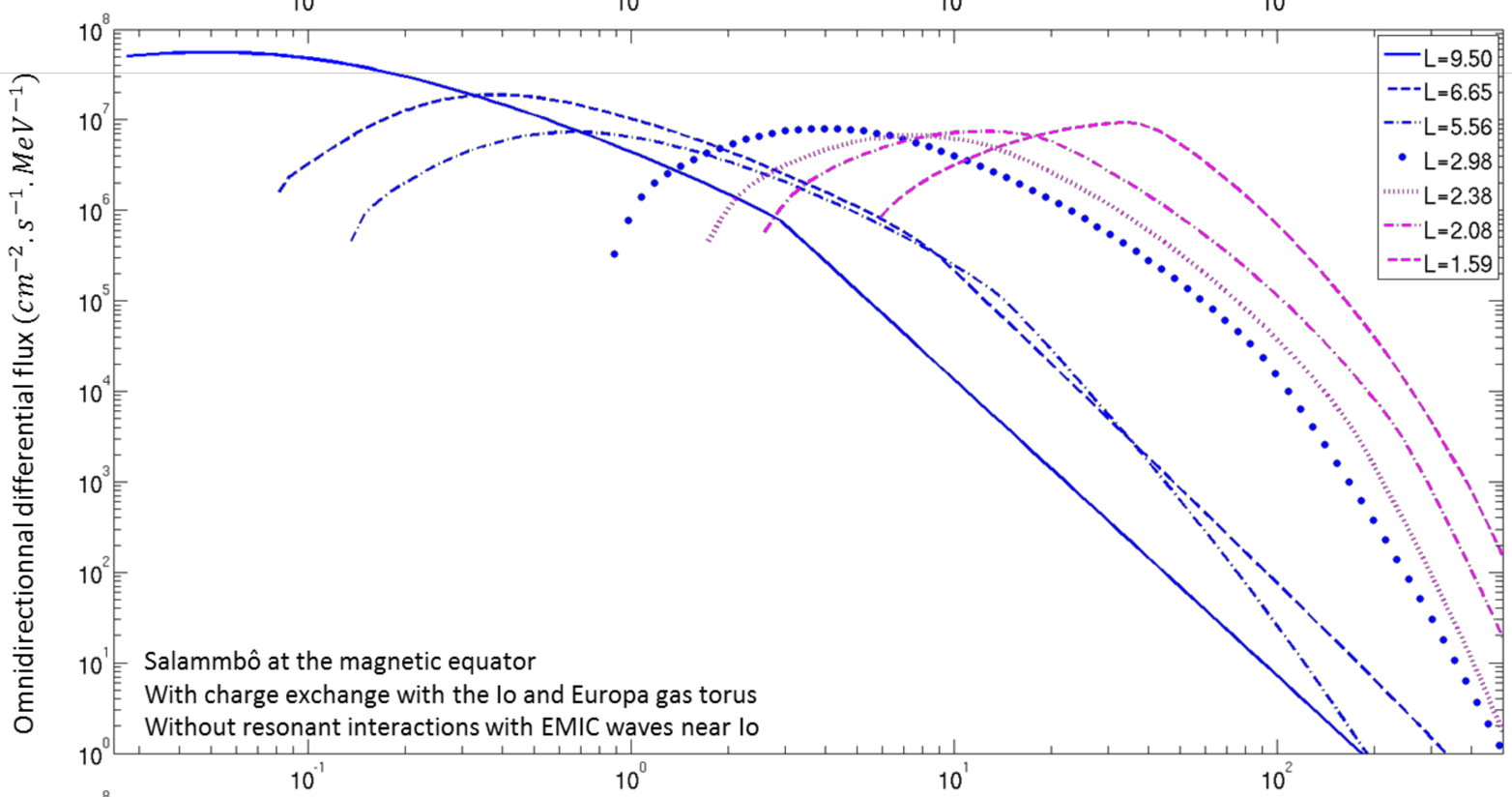
Omnidirectionnal differential flux (cm⁻².s⁻¹.MeV⁻¹)
L=9.50
L=6.65
L=5.56
L=2.98
L=2.38
L=2.08
L=1.59
Salammbô at the magnetic equator
With charge exchange with the Io and Europa gas torus
Without resonant interactions with EMIC waves near Io

d)

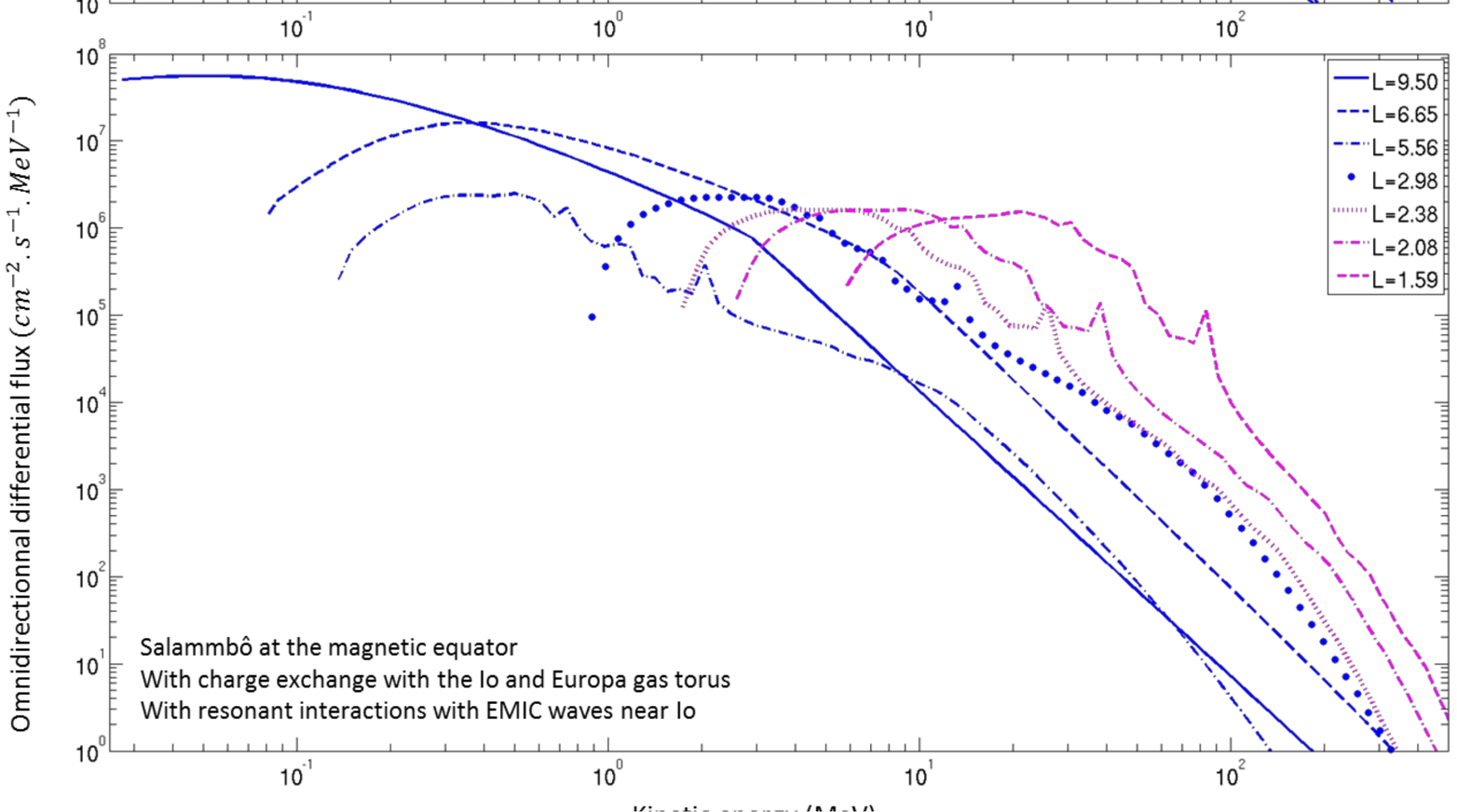
Omnidirectionnal differential flux (cm⁻².s⁻¹.MeV⁻¹)
L=9.50
L=6.65
L=5.56
L=2.98
L=2.38
L=2.08
L=1.59
Salammbô at the magnetic equator
With charge exchange with the Io and Europa gas torus
With resonant interactions with EMIC waves near Io
Kinetic energy (MeV)

Figure 8.

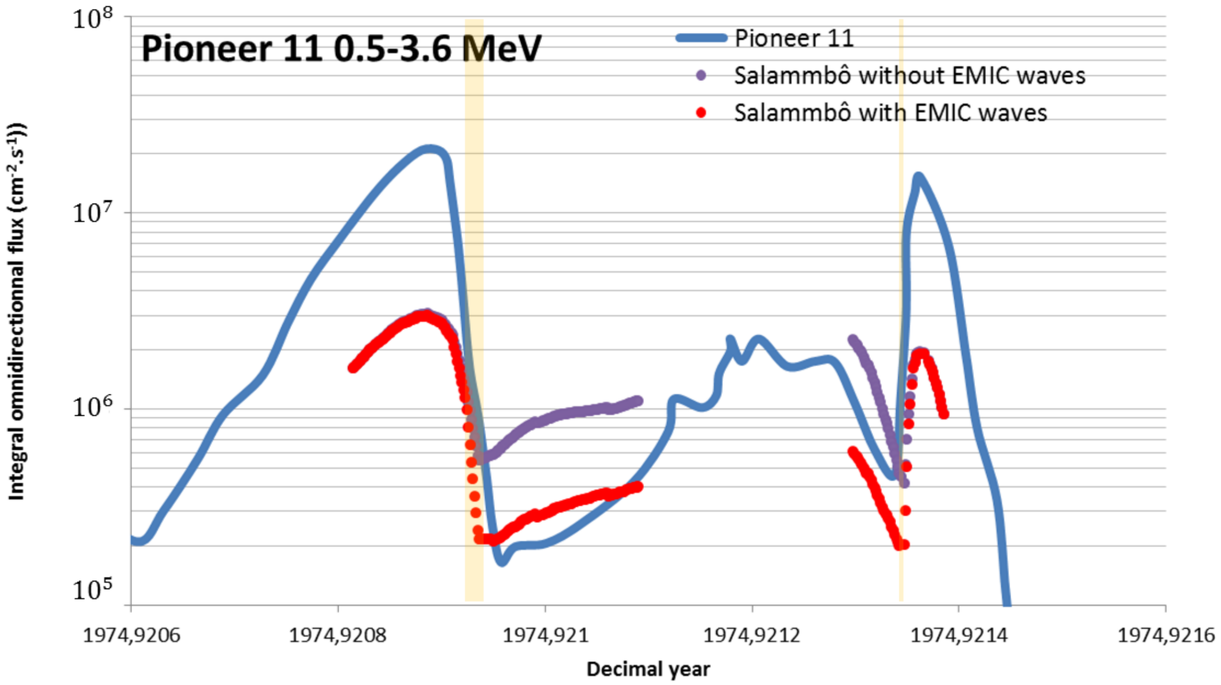
Pioneer 11 0.5-3.6 MeV
Pioneer 11
Salammbô without EMIC waves
Salammbô with EMIC waves
Integral omnidirectionnal flux (cm-2.s-1))
10^8
10^7
10^6
10^5
1974,9206
1974,9208
1974,921
1974,9212
1974,9214
1974,9216
Decimal year

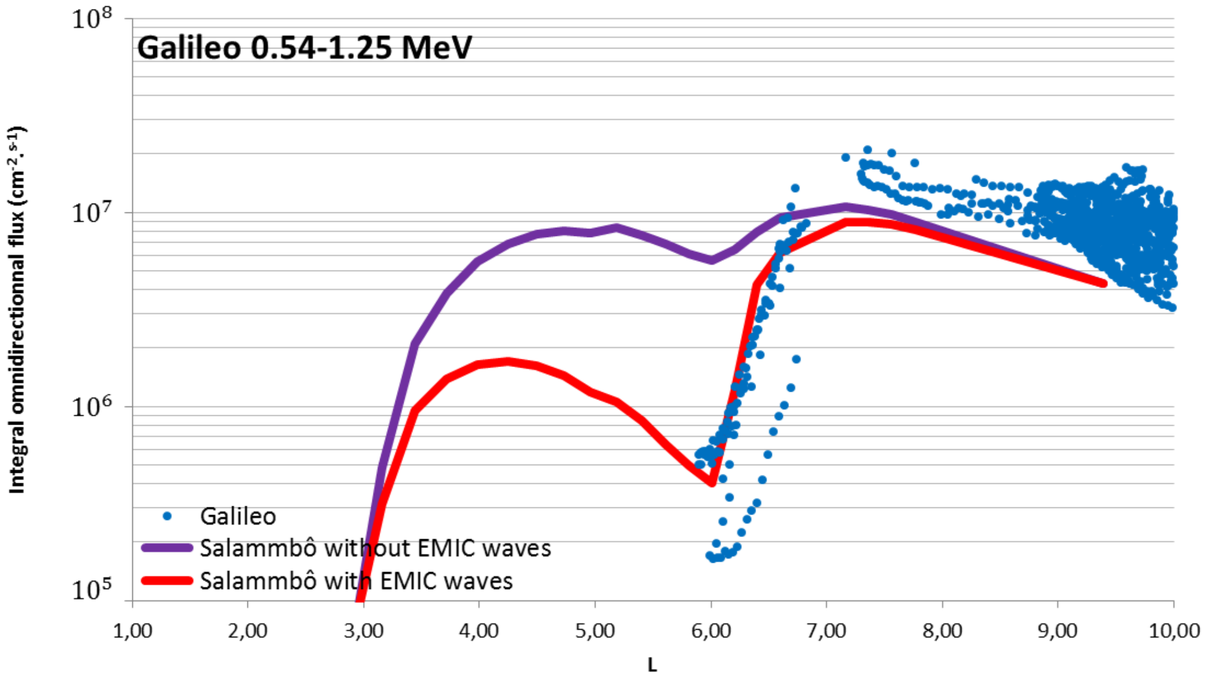
Galileo 0.54-1.25 MeV
Integral omnidirectionnal flux (cm-2.s-1)
10^8
10^7
10^6
10^5
Galileo
Salammbô without EMIC waves
Salammbô with EMIC waves
1,00
2,00
3,00
4,00
5,00
6,00
7,00
8,00
9,00
10,00
L

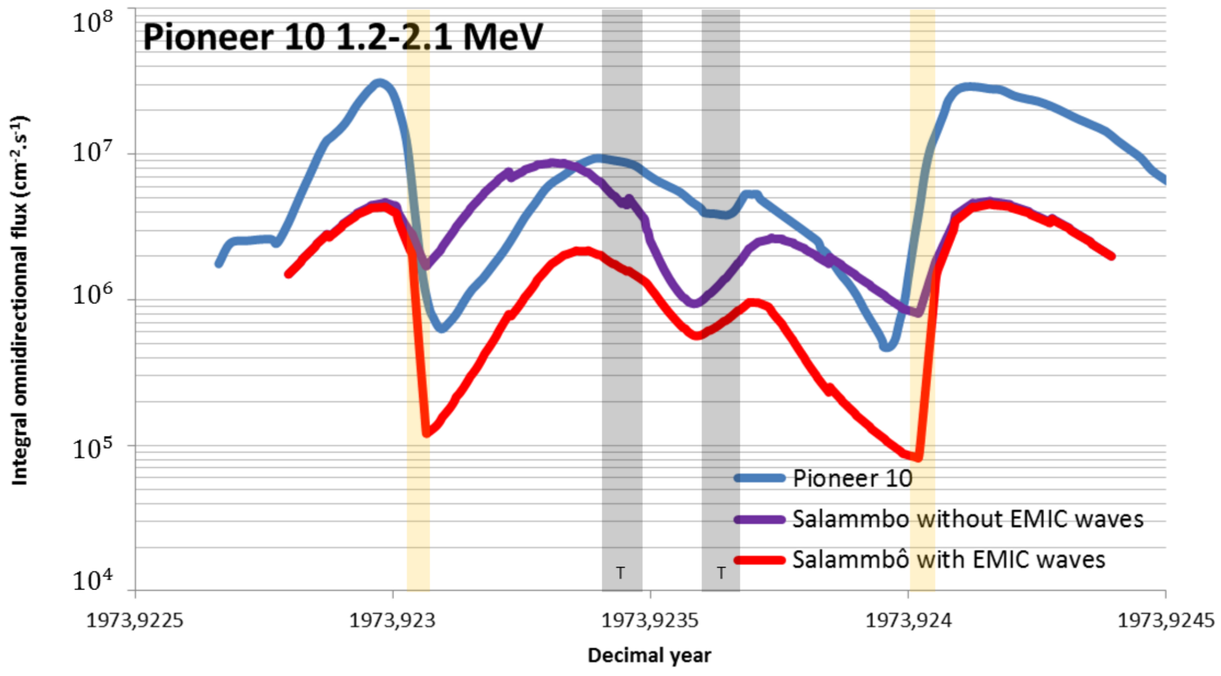
Pioneer 10 1.2-2.1 MeV
Integral omnidirectionnal flux (cm-2.s-1)
10^8
10^7
10^6
10^5
10^4
Pioneer 10
Salammbo without EMIC waves
Salammbô with EMIC waves
T
T
1973,9225
1973,923
1973,9235
1973,924
1973,9245
Decimal year

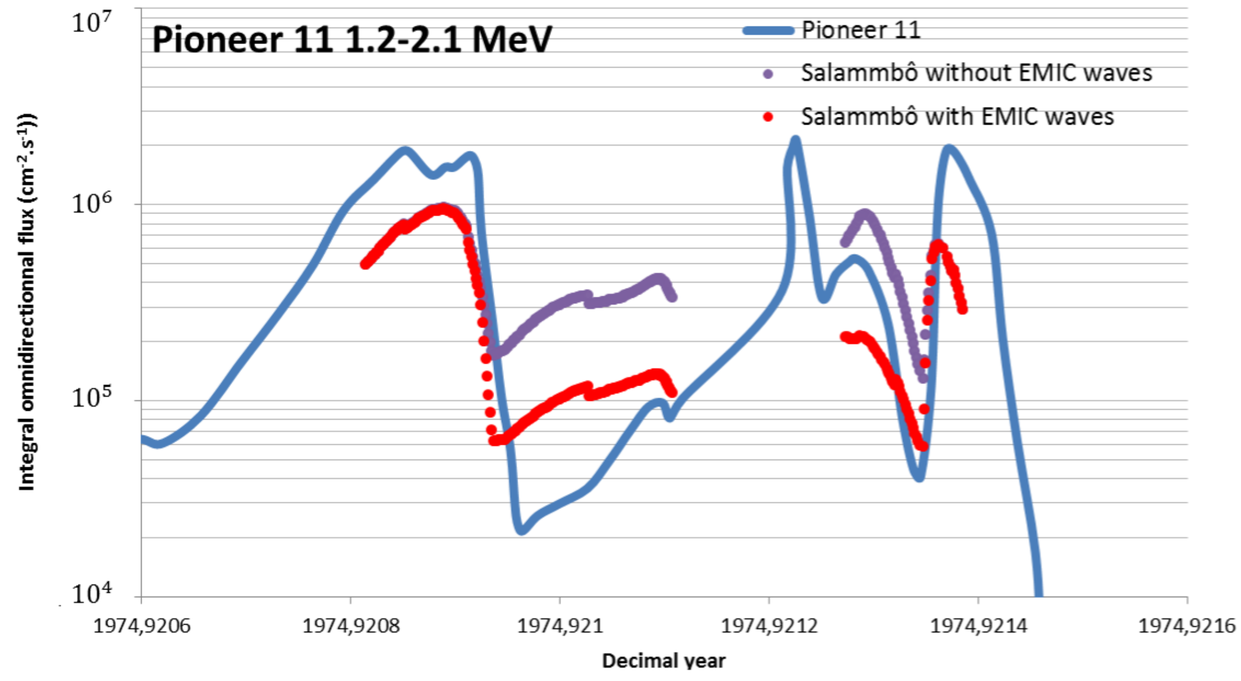
Pioneer 11 1.2-2.1 MeV
Pioneer 11
Salammbô without EMIC waves
Salammbô with EMIC waves
Integral omnidirectionnal flux (cm-2.s-1))
10^7
10^6
10^5
10^4
1974,9206
1974,9208
1974,921
1974,9212
1974,9214
1974,9216
Decimal year

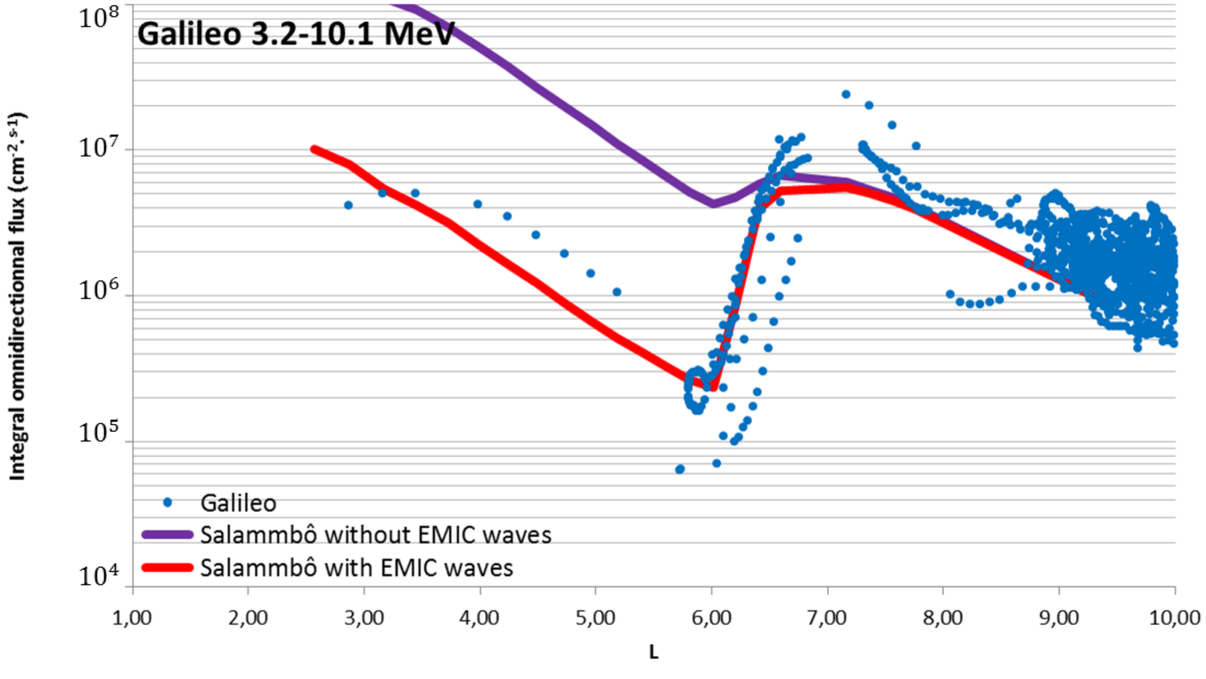
Galileo 3.2-10.1 MeV
Integral omnidirectionnal flux (cm-2.s-1)
10^8
10^7
10^6
10^5
10^4
Galileo
Salammbô without EMIC waves
Salammbô with EMIC waves
1,00
2,00
3,00
4,00
5,00
6,00
7,00
8,00
9,00
10,00
L

Figure 9.

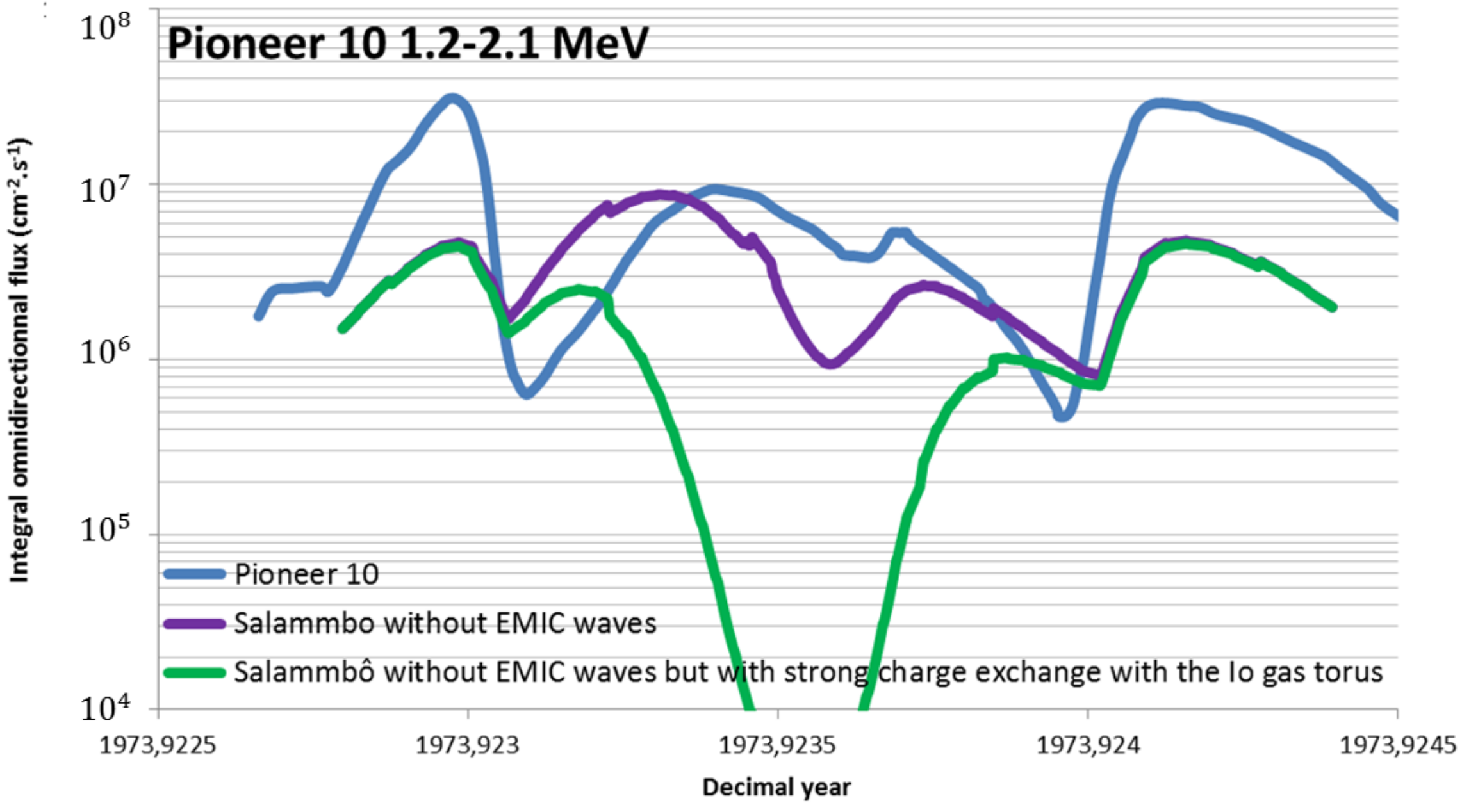
Pioneer 10 1.2-2.1 MeV
Integral omnidirectionnal flux (cm-2.s-1)
10^8
10^7
10^6
10^5
10^4
1973,9225
1973,923
1973,9235
1973,924
1973,9245
Decimal year
Pioneer 10
Salammbo without EMIC waves
Salammbô without EMIC waves but with strong charge exchange with the Io gas torus

Figure 10.

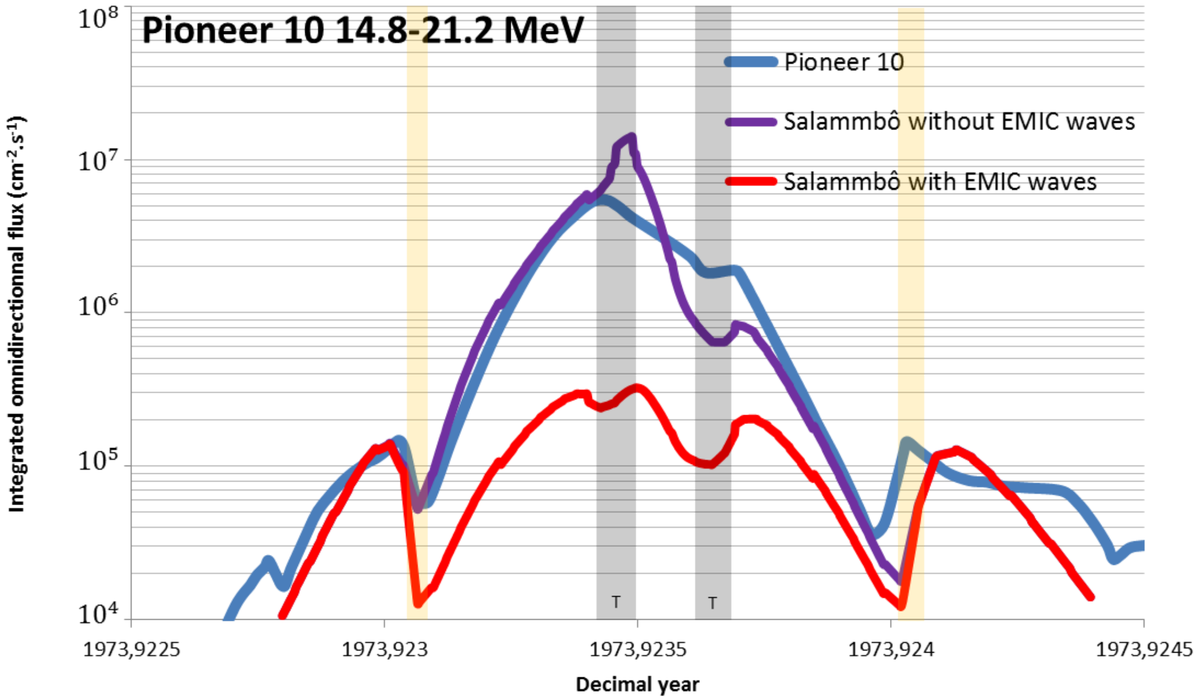
Pioneer 10 14.8-21.2 MeV
Pioneer 10
Salammbô without EMIC waves
Salammbô with EMIC waves
Integrated omnidirectionnal flux (cm-2.s-1)
Decimal year
T
T

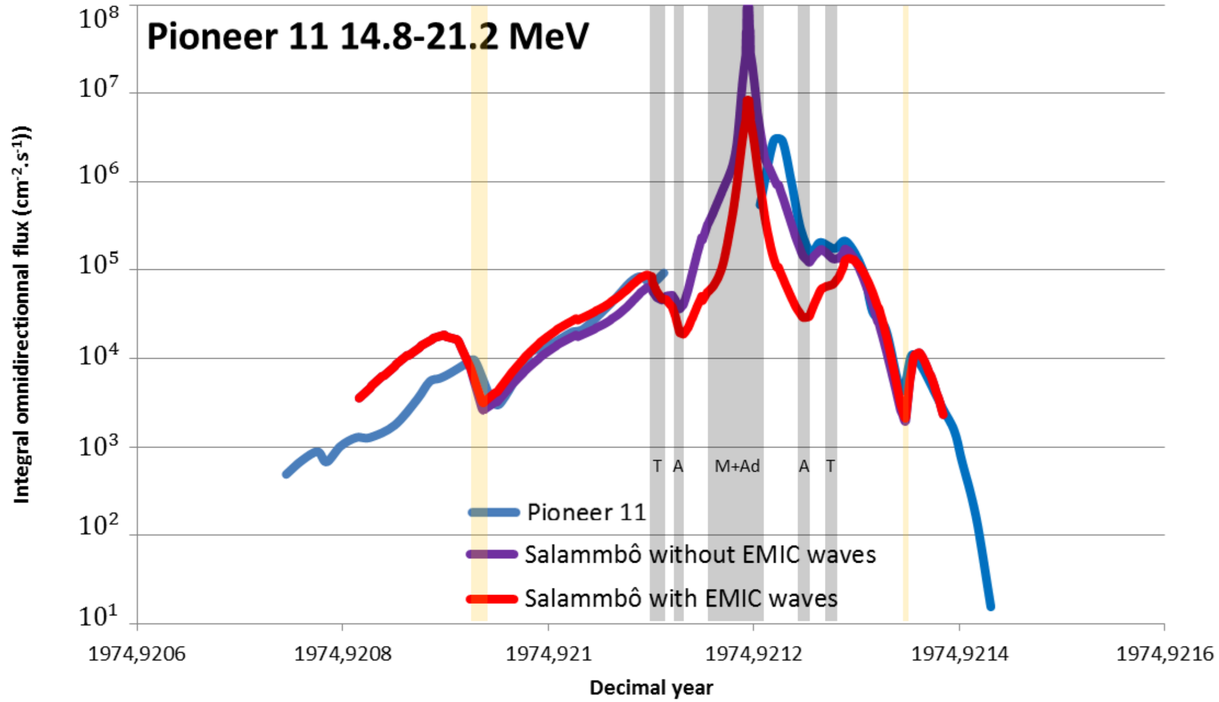
Pioneer 11 14.8-21.2 MeV
Pioneer 11
Salammbô without EMIC waves
Salammbô with EMIC waves
Integral omnidirectionnal flux (cm-2.s-1))
Decimal year
T A M+Ad A T

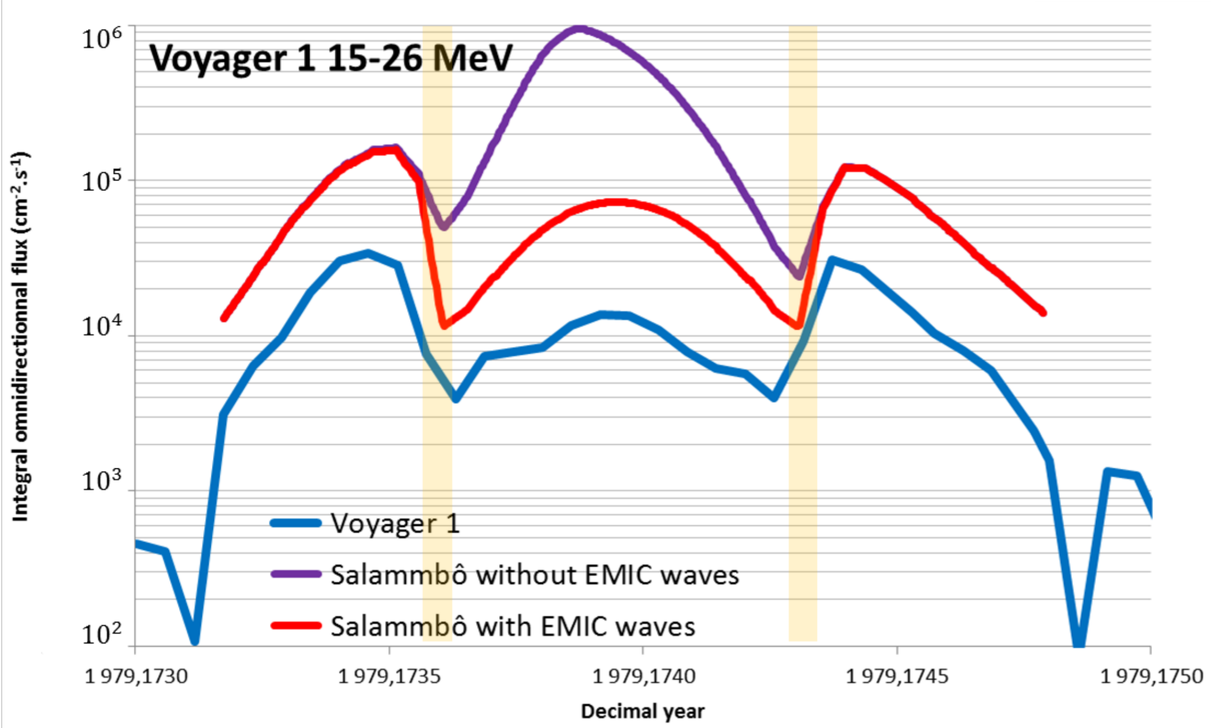
Voyager 1 15-26 MeV
Voyager 1
Salammbô without EMIC waves
Salammbô with EMIC waves
Integral omnidirectionnal flux (cm-2.s-1)
Decimal year

Figure 11.

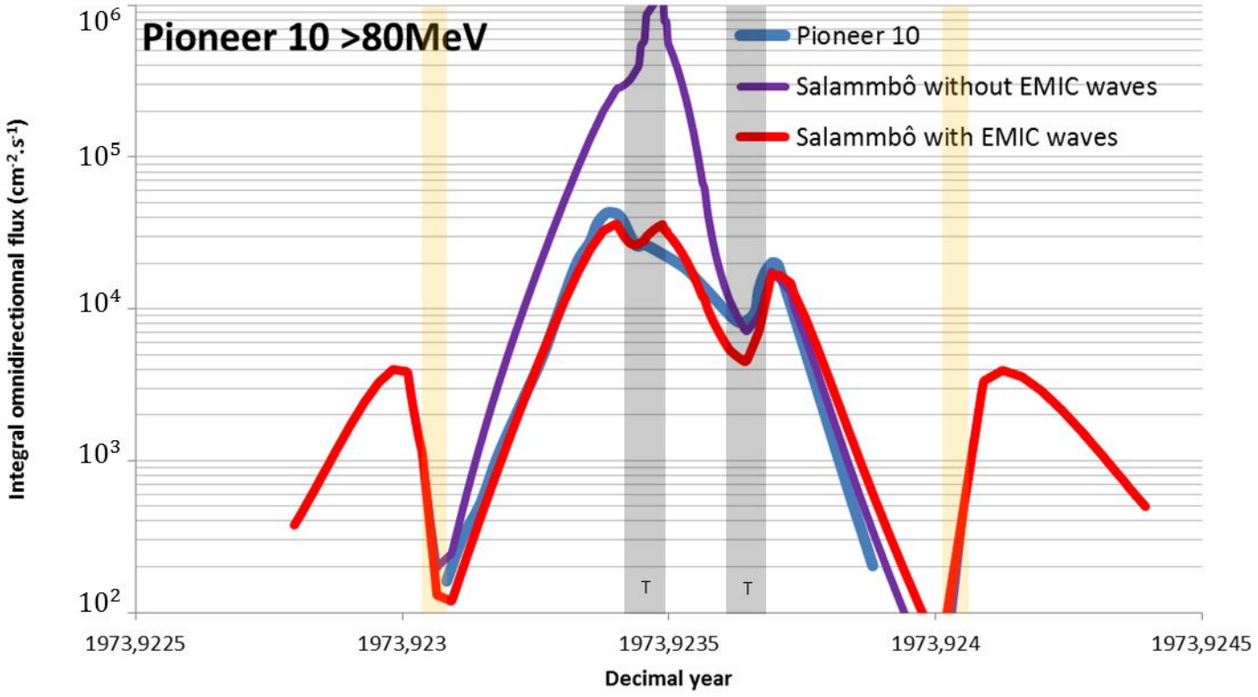
Pioneer 10 >80MeV
Pioneer 10
Salammbô without EMIC waves
Salammbô with EMIC waves
Integral omnidirectionnal flux (cm-2.s-1)
Decimal year
T
T

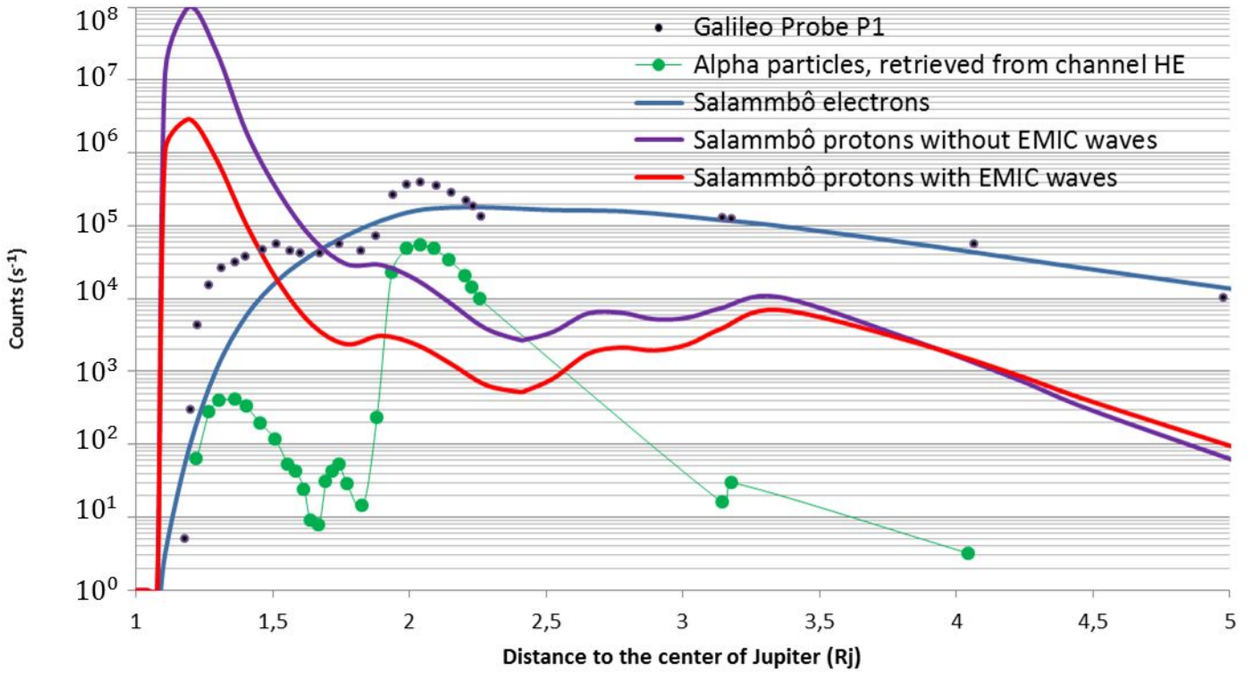
Galileo Probe P1
Alpha particles, retrieved from channel HE
Salammbô electrons
Salammbô protons without EMIC waves
Salammbô protons with EMIC waves
Counts (s-1)
Distance to the center of Jupiter (Rj)

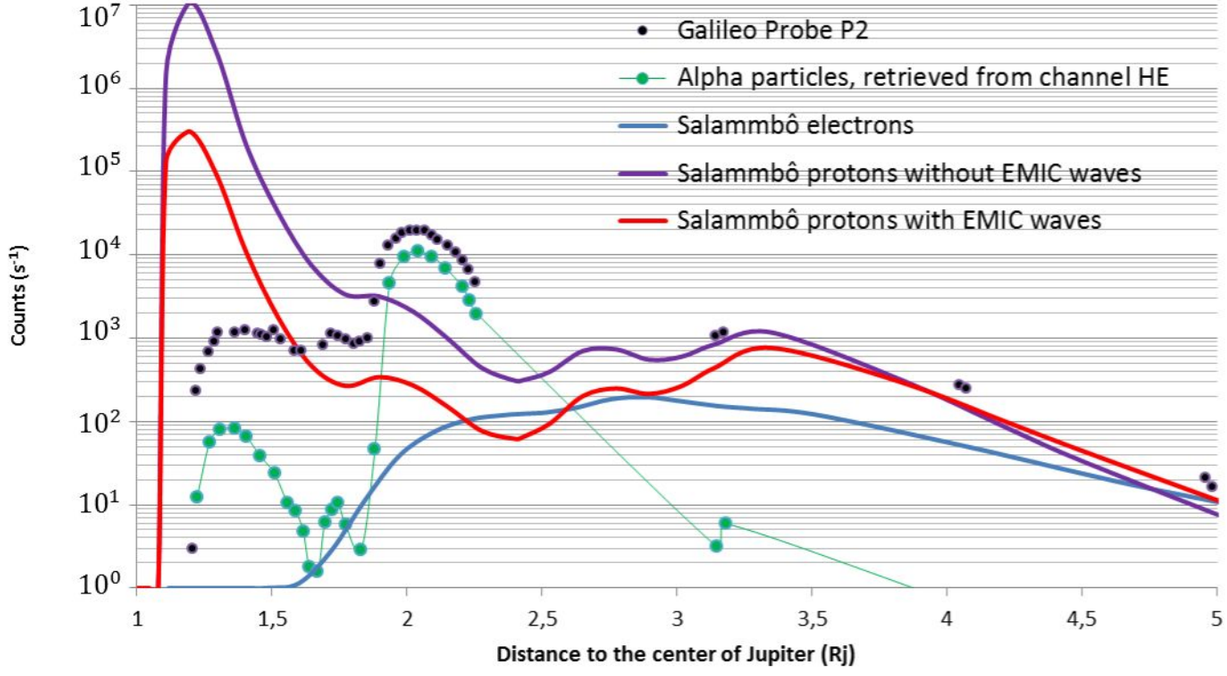
Galileo Probe P2
Alpha particles, retrieved from channel HE
Salammbô electrons
Salammbô protons without EMIC waves
Salammbô protons with EMIC waves
Counts (s-1)
Distance to the center of Jupiter (Rj)

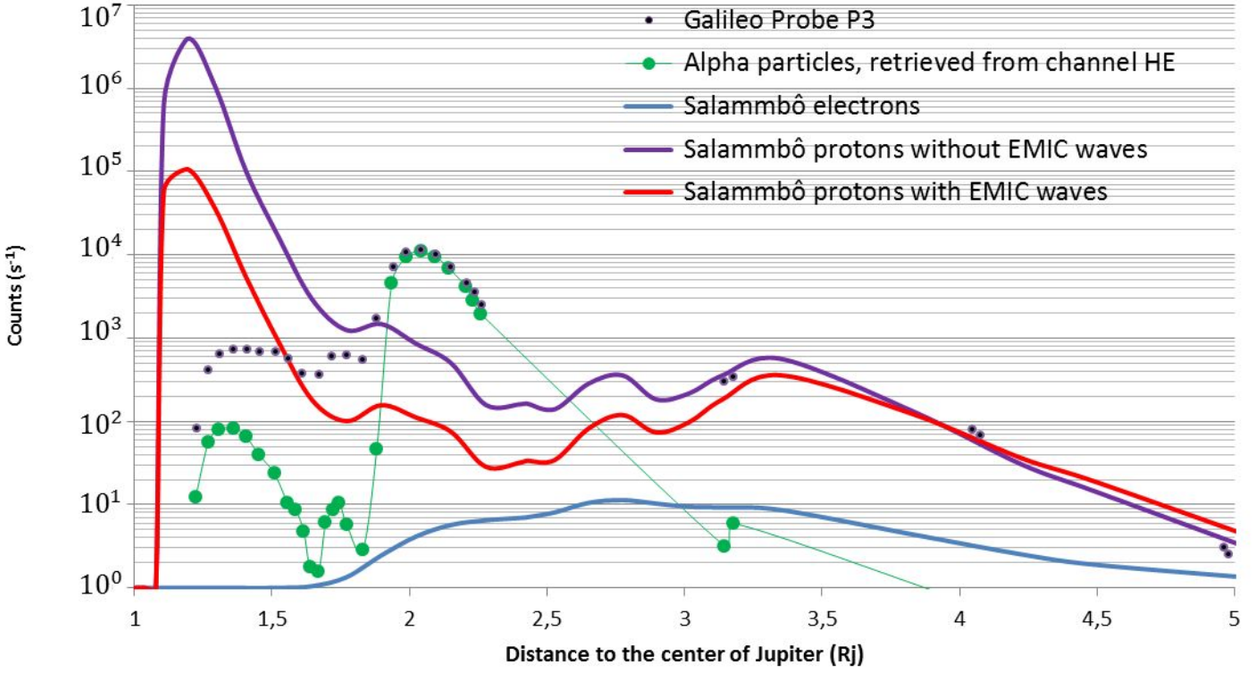
Galileo Probe P3
Alpha particles, retrieved from channel HE
Salammbô electrons
Salammbô protons without EMIC waves
Salammbô protons with EMIC waves
Counts (s-1)
Distance to the center of Jupiter (Rj)

Figure A1.

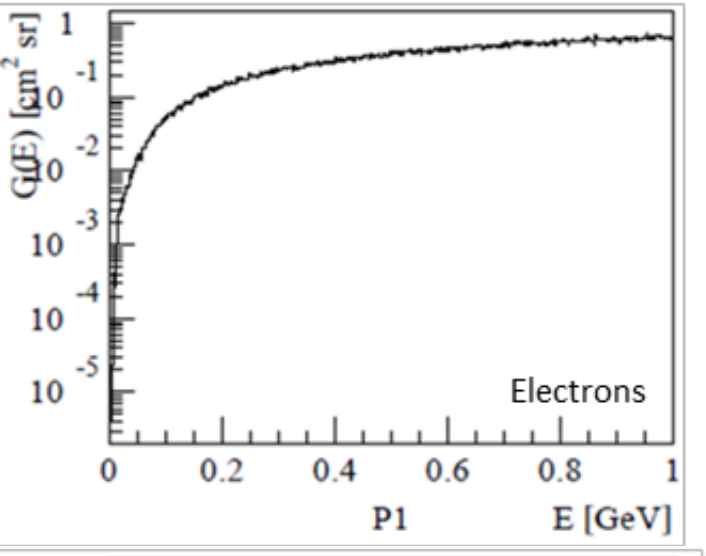
G(E) [cm² sr]
Electrons
P1
E [GeV]

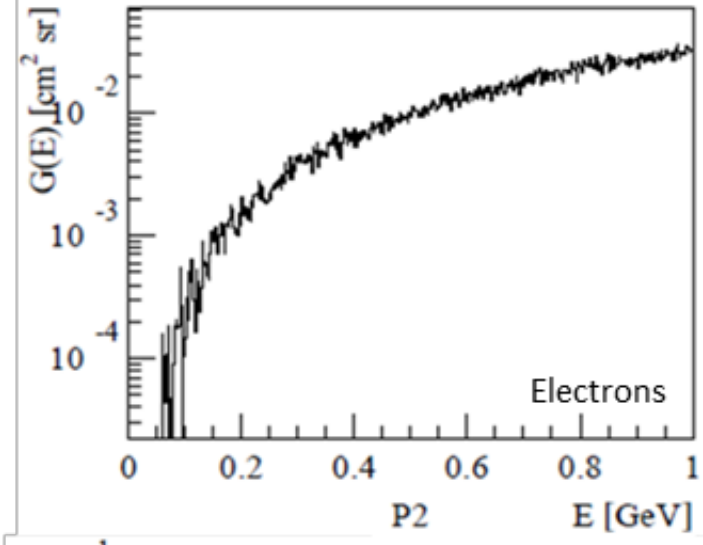
G(E) [cm² sr]
Electrons
P2
E [GeV]

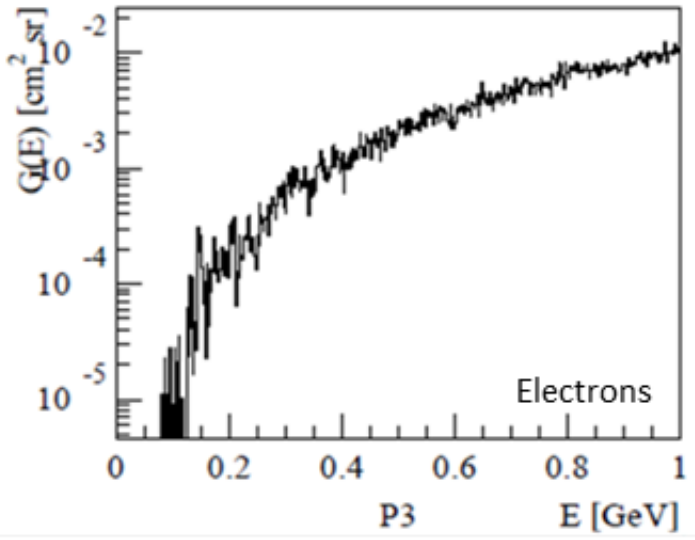
G(E) [cm² sr]
Electrons
P3
E [GeV]

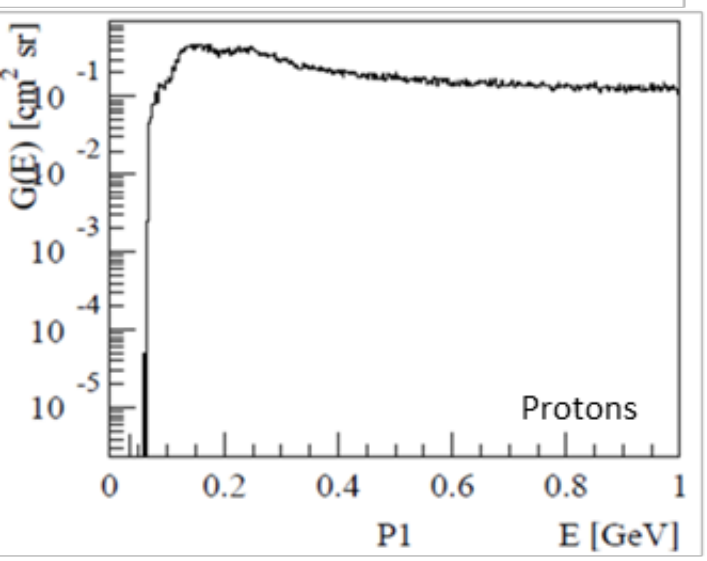
G(E) [cm² sr]
Protons
P1
E [GeV]

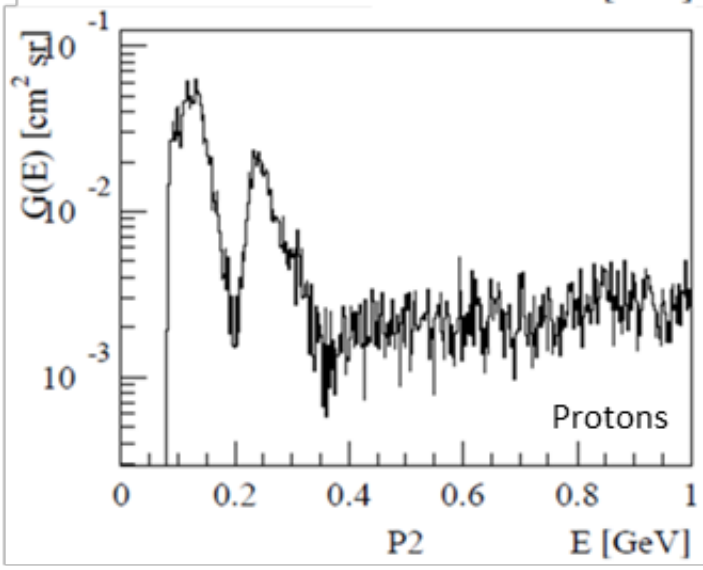
G(E) [cm² sr]
Protons
P2
E [GeV]

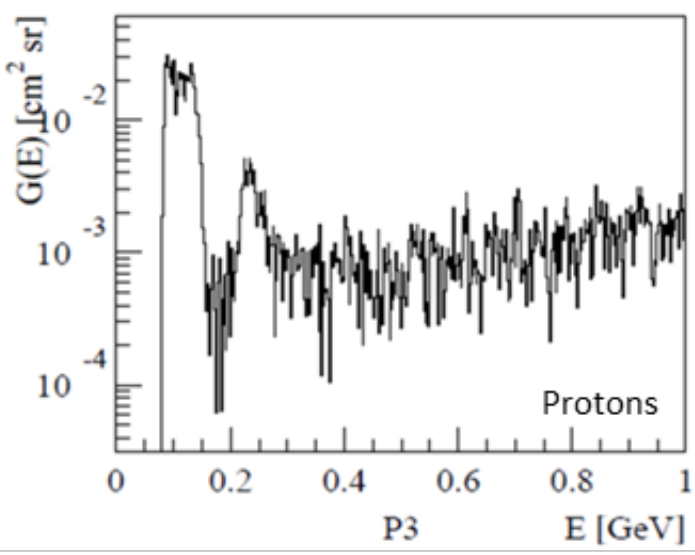
G(E) [cm² sr]
Protons
P3
E [GeV]

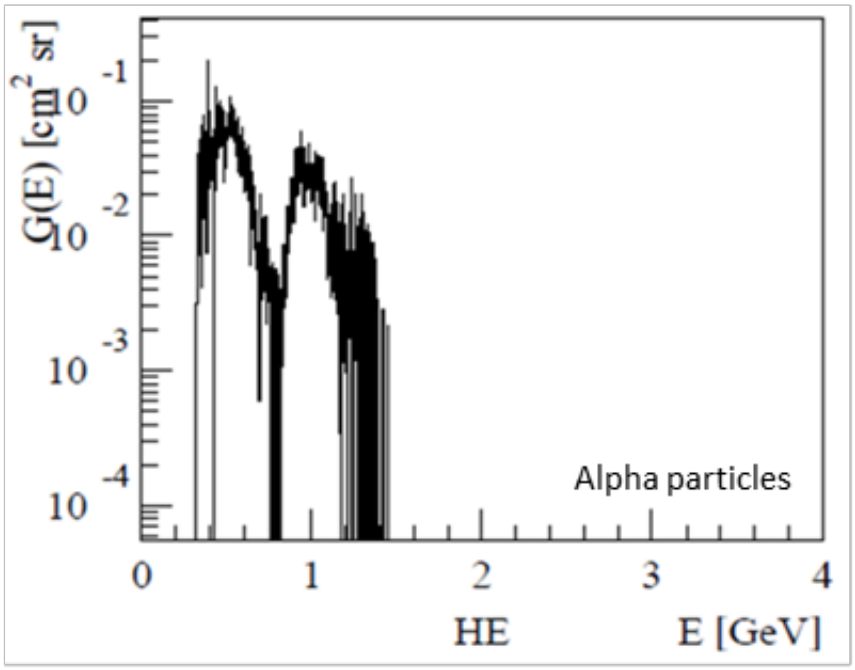
G(E) [cm² sr]
Alpha particles
HE
E [GeV]

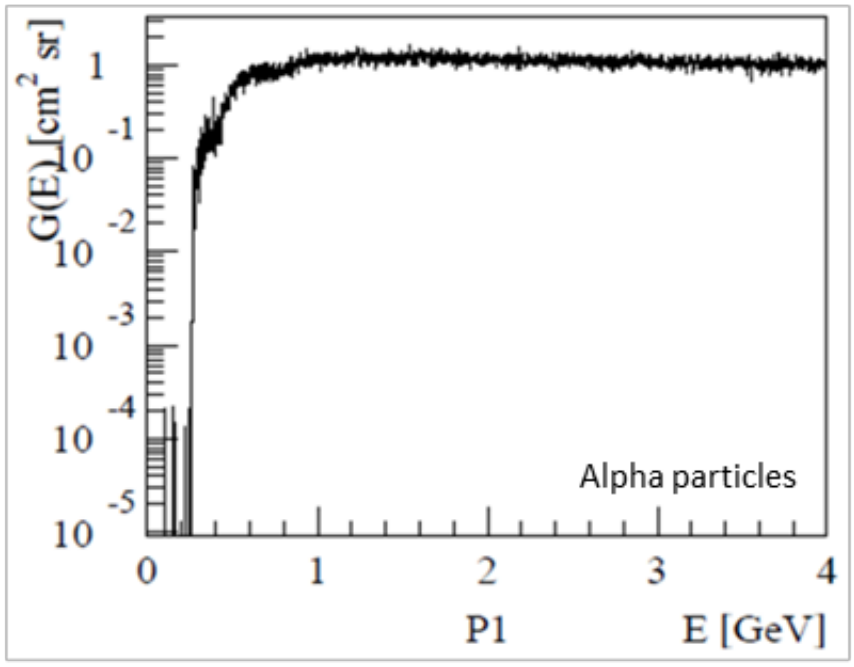
G(E) [cm² sr]
Alpha particles
P1
E [GeV]

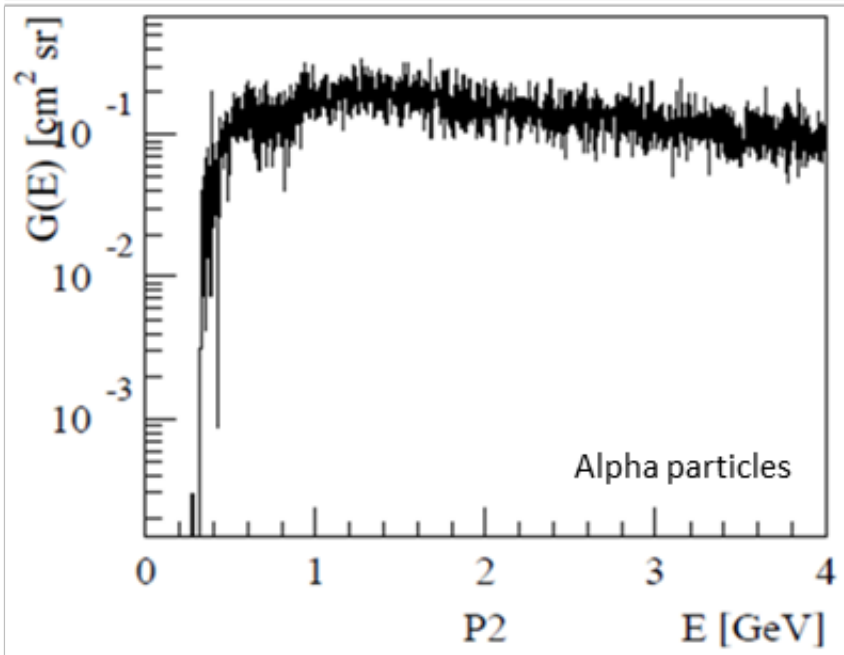
G(E) [cm² sr]
Alpha particles
P2
E [GeV]

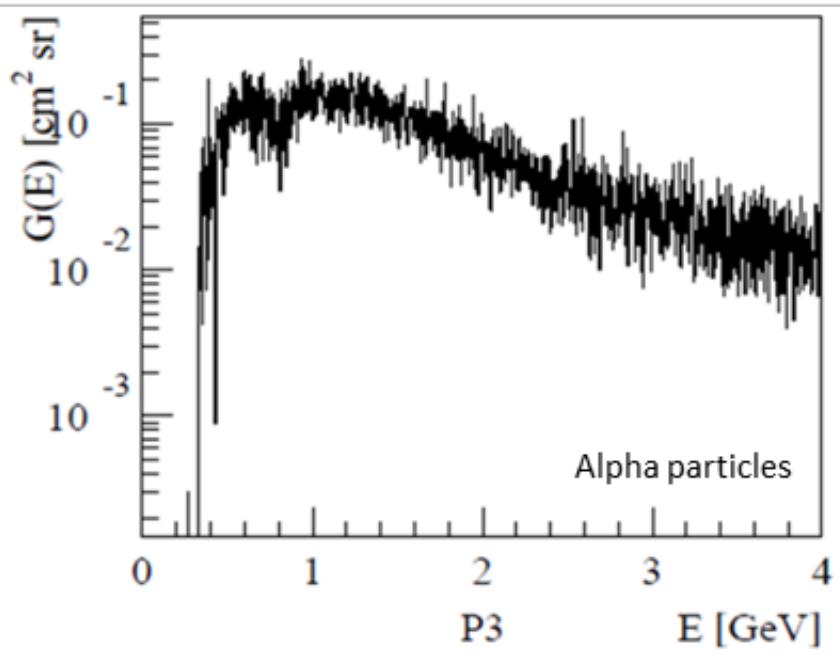
G(E) [cm² sr]
Alpha particles
P3
E [GeV]

973 Warnecke J., M. G. Kivelson, K. K. Khurana, D. E. Huddleston and C. T. Russell (1997), Ion
974 cyclotron waves observed at Galileo's Io encounter: Implications for neutral cloud distribution
975 and plasma composition, Geophys. Res. Lett. 24, doi: 10.1029/97GL01129
976 Williams, D., R. McEntire, S. Jaskulek, and B. Wilken (1992), The Galileo Energetic
977 Particles Detector, Space Science Reviews, 60(1-4), doi:10.1007/bf00216863
978 Woodfield, E. E., R. B. Horne, S. A. Glauert, J. D. Menietti, and Y. Y. Shprits (2014), The
979 origin of Jupiter's outer radiation belt, J. Geophys. Res. Space Physics, 119(5), 3490-3502,
980 doi:10.1002/2014JA019891
981
982
983
984
985
986
987
988
989
990
991
992